Queuing Models With Applications to Mode Selection in Device-to-Device Communications Underlaying Cellular Networks

Lei Lei, *Member, IEEE*, Xuemin (Sherman) Shen, *Fellow, IEEE*, Mischa Dohler, *Fellow, IEEE*, Chuang Lin, *Senior Member, IEEE*, and Zhangdui Zhong

***Abstract*—In this paper, we study the performance of mode selections in device-to-device (D2D) communications in terms of end-to-end average throughput, average delay, and dropping probability, considering dynamic data arrival with non-saturated buffers. We first introduce a general framework that includes three canonical routing modes, namely D2D mode, cellular mode, and hybrid mode, which can be combined with different resource allocation restrictions to represent the semi-static and dynamic selections of the three resource sharing modes. A queuing model is developed when the routing mode for every D2D connection is chosen, and an exact numerical analysis and an approximate decomposition and iteration approach are proposed. The performance measures are obtained from the decomposition approach and validated by means of simulation. We further introduce a mode selection scheme that adaptively chooses to semi-statically or dynamically select the resource sharing modes according to the estimated performance measures.**

***Index Terms*—Device-to-device communication, mode selection, queuing models.**

I. Introduction

DEVICE-TO-DEVICE (D2D) communications commonly refer to technologies that enable devices to communicate directly with each other in a single hop or along routes without the need of an infrastructure, e.g., access points or base stations. In recent years, mobile operators and vendors are exploring the possibilities of introducing D2D function in cellular networks [1]–[4], which is envisioned to provide better Quality-of-Service (QoS) guarantees to the users than traditional D2D technologies (e.g., Bluetooth and WiFi). This is due to the better controllable interference in the licensed bands [3] and more efficient radio resource management with the help of the base station (BS). Although the problem of cross-layer performance modeling and analysis of conventional cellular networks and wireless multihop networks has been addressed in the literature [5]–[7], the analysis and optimization of more realistic D2D communications underlaying cellular networks with dynamic arrival and departure of packets with non-saturated buffer is an open research problem [8].

In D2D communications, mode selection is one of the key research problems, which chooses one of the three resource sharing modes (RSMs) for a pair of D2D users within direct communications range [9]: 1) D2D mode with non-orthogonal sharing (NOS) in which D2D users communicate directly reusing the same resources with the cellular users, 2) D2D mode with orthogonal sharing (OS) in which D2D users communicate directly and use dedicated resources, 3) cellular mode (CM) in which D2D users communicate via the BS. Mode selection can be performed either semi-statically at the time-scale of connection establishment/release, or dynamically per time slot [2]. Dynamic mode selection can capture and utilize the fast fading effects of wireless channels opportunistically, while semi-static mode selection has the advantage of saving computation and communication overhead. Compared with the simple mode selection algorithms which use only the received signal strength over the links or the distance between the devices as mode selection criteria, recent research work on D2D communications propose to make mode selection decision based on the system performance in terms of throughput or power, which are estimated assuming the optimum power control and resource allocation algorithms are adopted under the above three resource sharing modes [9]–[13]. The main difference between the semi-static and dynamic mode selection algorithms lies in whether the long-term time-average throughput/power or instantaneous throughput/power per time slot is used as the selection criteria, where the former is obtained by considering the channel gains comprising only the path loss attenuation, while the latter is obtained with the channel gains capturing both the path loss and fast fading effects. Most of the mode selection algorithms in literature consider either the semi-static or dynamic time-scale without comparing the performance gap between the two methods.

Existing work on mode selection in D2D communications usually assumes that the D2D and cellular users are saturated with infinite backlogs, while in reality data will arrive to the

Manuscript received November 26, 2013; revised April 16, 2014; accepted June 29, 2014. Date of publication July 8, 2014; date of current version December 8, 2014. This work was supported in part by the National Basic Research Program of China (973 Program) under Grant 2010CB328105, by the National Natural Science Foundation of China under Grants 61272168 and U1334202, by the State Key Laboratory of Rail Traffic Control and Safety in Beijing Jiaotong University under Contract RCS2014ZT10. The associate editor coordinating the review of this paper and approving it for publication was Y. Chen.

L. Lei and Z. Zhong are with the State Key Laboratory of Rail Traffic Control and Safety, Beijing Jiaotong University, Beijing 100044, China.

X. Shen is with the Department of Electrical and Computer Engineering, University of Waterloo, Waterloo, ON N2L 3G1, Canada.

M. Dohler is with Centre for Telecommunications Research Department of Informatics, King's College London, London, WC2R 2LS, U.K.

C. Lin is with the Department of Computer Science and Technology, Tsinghua University, Beijing 100084, China.

Color versions of one or more of the figures in this paper are available online at http://ieeexplore.ieee.org.

Digital Object Identifier 10.1109/TWC.2014.2335734

users according to a dynamic process. In semi-static mode selection algorithms, typical QoS metrics such as delay and dropping probability cannot be estimated and used as the mode selection criteria under the infinite backlog assumption, since these metrics depend on the queuing dynamics at each user, which in turn depends on the traffic arrival pattern. In dynamic mode selection algorithms, mode selection is performed jointly with resource allocation, which is responsible for selecting the set of links for data transmissions at the beginning of each time slot. Related work on dynamic mode selection and resource allocation [11], [13] mainly focus on the interference control and management between D2D links and cellular links such that they can efficiently reuse the radio resources whenever the interference is small; the optimization objectives are mostly throughput maximization or power minimization. However, existing research on resource allocation and scheduling in wireless networks [15], [16] show that algorithms optimized under the infinite backlog traffic model considering only the channel state information are *not* sufficient to ensure queue stability or guarantee packet delay/QoS requirement under the dynamic packet arrival setting. Therefore, the queue state information should *also* be taken into account.

The introduction of D2D communications may bring three potential intracell interference scenarios into cellular networks depending on the radio resource reuse restrictions: (1) interference between multiple D2D users; (2) interference between a cellular user and a D2D user; (3) interference between a cellular user and multiple D2D users. Interference scenario (1) arises when the same set of resource blocks are allocated to multiple D2D users, while the interference between D2D users and cellular users are avoided by statically or semi-statically allocating a group of dedicated resources to all the D2D users at the cost of reduced spectrum efficiency. Interference scenarios (2) and (3) arise when the resource blocks allocated to a cellular user are reused by one (scenario (2)) or more (scenario (3)) D2D users. Existing work on mode selection under the infinite backlog assumption mostly assumes the interference scenario (2) [9], [10], [12], [14], which imposes the restriction that the resources allocated to a cellular user can be reused by at most one D2D user, although some recent literature begins to address the mode selection problem under interference scenario (3) without the above resource allocation restriction [11]. This is largely because interference scenario (2) is more simple and implementable compared with interference scenario (3). In this paper, we consider a dynamic packet arrival setting, and focus on the interference scenario (2) similar to most related research work under infinite backlog assumption, which will limit the system state space of the Discrete Time Markov Chain (DTMC) underlying our queuing model. Extending our work to the interference scenario (3) will be an interesting and challenging topic for future study.

In this paper, we define three routing modes for a D2D user pair that can characterize both the semi-static and dynamic selections of the above three resource sharing modes by setting different resource allocation restrictions. The exact queuing model for D2D communications underlaying cellular networks is developed when the routing mode for every D2D connection is chosen, considering the dynamic packet arrival process and the fast fading wireless channels under potential interference with adaptive modulation and coding (AMC) in the physical layer. An exact numerical analysis is proposed for the queuing model, where different categories of scheduling algorithms with/without the channel and queue states information can be included to describe the resource allocation methods in semi-static mode selection or the joint dynamic mode selection and resource allocation methods. We construct Discrete Time Markov Chains (DTMC) underlying the queuing model where every state is a tuple consisting of the queue states and the channel states of the links that may be scheduled to serve the queues. We derive the formula for computing the state transition probabilities of the DTMC, which can be used to calculate the stationary distributions using balance equation. Due to the large state space and computational complexity of the exact model, we use model decomposition and iteration technique [17], [18] to decompose the exact queuing model into submodels with inter-correlated service rates. We derive the equations for computing the approximated state transition probabilities of the DTMCs underlying the decomposed submodels so that the approximate stationary distributions can be determined. Finally, we provide the formulas for obtaining the performance measures such as end-to-end average throughput, average delay and packet dropping probability based on the derived approximate stationary distributions. We develop a mode selection method based on the system performance measures derived from numerical analysis, which makes a flexible decision on whether mode selection should be performed semi-statically or dynamically for a D2D user pair to achieve the best tradeoff between efficiency and complexity.

The remainder of the paper is organized as follows. In Section II, the system model is described. The queuing model is presented in Section III, along with the formal description of scheduling algorithms taking MaxWeight as an example. In Section IV, the exact numerical analysis method and the model decomposition and iteration method are proposed to derive the exact and approximate system performance. The numerical results are verified by means of simulations in Section IV, and the application of the proposed numerical method for mode selection is discussed. Finally, conclusions are given in Section VI with discussion on future work. Since many symbols are used in this paper, Table I summarizes the most important ones.

II. Network Model

A. Nodes, Links, and Connections

We consider a general network model with a set $\mathcal{N}$ of nodes and a set $\mathcal{L}$ of transmission links. Define $\mathcal{N} := \{0, 1, \ldots, N\}$, where node 0 represents the base station (BS) and nodes $1, \ldots, N$ represent the UEs. Let $\mathcal{N}_{\mathrm{D}} := \{1, \ldots, 2D\}$ be the set of D2D UEs (DUEs) of the D D2D pairs, where nodes $2i-1$ and $2i$ denote the source (src.) and destination (dest.) DUEs of pair i ($i \in \{1, \ldots, D\}$), respectively. Denote the sets of src. DUEs and dest. DUEs as $\mathcal{N}_{\mathrm{Ds}} := \{1, 3, \ldots, 2D-1\}$ and $\mathcal{N}_{\mathrm{Dd}} := \{2, 4, \ldots, 2D\}$, respectively. Let $\mathcal{N}_{\mathrm{Cu}} := \{2D+1, \ldots, 2D+C_{\mathrm{u}}\}$ be the set of C_{u} uplink Cellular UEs (CUEs), and $\mathcal{N}_{\mathrm{Cd}} := \{2D+C_{\mathrm{u}}+1, \ldots, 2D+C_{\mathrm{u}}+C_{\mathrm{d}}\}$ be the set of

TABLE I
SUMMARY OF IMPORTANT SYMBOLS USED

Category	Symbol	Definition
Constant	D	The number of D2D UE pairs
	C_{u}	The number of cellular UEs with uplink communications
	C_{d}	The number of cellular UEs with downlink communications
	C	The number of connections
	L	The number of eligible links
	N_{Q}	The queue capacity in number of bits or packets
Set	$\mathcal{N}$	The set of nodes i, $\mathcal{N} := \{0, 1, ..., N\} = \{0\} \bigcup \mathcal{N}_{\mathrm{D}} \bigcup \mathcal{N}_{\mathrm{Cu}} \bigcup \mathcal{N}_{\mathrm{Cd}}$
	$\mathcal{N}_{\mathrm{D}}$	The set of D pairs of DUEs, $\mathcal{N}_{\mathrm{D}} := \{1, \ldots, 2D\}$
	$\mathcal{N}_{\mathrm{Cu}}$	The set of C_{u} uplink CUEs, $\mathcal{N}_{\mathrm{Cu}} := \{2D+1, \ldots, 2D+C_{\mathrm{u}}\}$
	$\mathcal{N}_{\mathrm{Cd}}$	The set of C_{d} downlink CUEs, $\mathcal{N}_{\mathrm{Cd}} := \{2D+C_{\mathrm{u}}+1, \ldots, 2D+C_{\mathrm{u}}+C_{\mathrm{d}}\}$
	$\mathcal{L}$	The set of transmission links (i,j), $\mathcal{L} := \mathcal{L}_{\mathrm{D}} \bigcup \mathcal{L}_{\mathrm{Cu}} \bigcup \mathcal{L}_{\mathrm{Cd}}$
	$\mathcal{C}$	The set of connections $\mathcal{C} := \{1, \ldots, C\} = \mathcal{C}_{\mathrm{D}} \bigcup \mathcal{C}_{\mathrm{Cu}} \bigcup \mathcal{C}_{\mathrm{Cd}}$
	$\mathcal{L}_c$	The set of all links (i,j) that connection c data is allowed to use
	$\widetilde{\mathcal{L}}$	The set of eligible links when the routing modes are determined for every D2D connection, $\widetilde{\mathcal{L}} := \sum_{c \in \mathcal{C}} \mathcal{L}_c$
	Θ	The set of queues in the system
	$\mathcal{B}_u$	A RRG, which is a set of links that can be scheduled for transmission simultaneously
	$\mathcal{U}$	The index set of RRGs, $\mathcal{U} = \{\mathcal{U}_{\mathrm{u}}, \mathcal{U}_{\mathrm{d}}\}$
	$\mathcal{U}_*$	Represents $\mathcal{U}_{\mathrm{u}}$ or $\mathcal{U}_{\mathrm{d}}$, which is the index set of uplink or downlink RRGs
	$\mathcal{U}_{ij}$	The index set of RRGs that contain link (i,j), $\mathcal{U}_{ij} := \{u \vert (i,j) \in \mathcal{B}_u, u \in \mathcal{U}\}$
Variable	(i,j)	A transmission link from node i to node j
	$A_{c,t}$	The amount of new connection c data arrived to its source node during time slot t
	$q_i^{(c)}$	The queue maintained at node i for connection c
	$Q_{i,t}^{(c)}$	The length of $q_i^{(c)}$ at the beginning of time slot t
	$x_{u,t}$	The scheduling result for RRG $\mathcal{B}_u$ at time slot t, $x_{u,t}^{(m)} \in \{0,1\}$
	$r_{i,t}^{(c)}$	The instantaneous data rate of queue $q_i^{(c)}$ during time slot t
	$r_{ij,t}^{(u)}$	The instantaneous data rate of link (i,j) when RRG $\mathcal{B}_u$ is scheduled
	I_{ij}	The potential interfering link from the transmitter of node i to the receiver of node j
	$SINR_{ij,t}^{(u)}$	The instantaneous SINR of link (i,j) when RRG $\mathcal{B}_u$ is scheduled
	$\gamma_{ij,t}$	The (virtual) SNR of the wireless channel between the transmitter of node i and the receiver of node j at time slot t
	$A_{i,t}^{(c)}$	The number of packets arrived to node i for connection c during the time slot t
	$\mathbf{a}_*$	Represents $\mathbf{a}_{\mathrm{u}}$ or $\mathbf{a}_{\mathrm{d}}$, which is the uplink or downlink scheduling action, $\mathbf{a}_* := \{x_u \in \{0,1\} \vert u \in \mathcal{U}_*\}$
	$\phi_{\mathbf{S}}(\mathbf{a}_*^{(u)})$	The selection probability of RRG $\mathcal{B}_u$ by the uplink or downlink scheduler when the system state is $\mathbf{S}$
State	$\mathbf{S}_t$	The global system state at time slot t, $\mathbf{S}_t = (\mathbf{H}_t, \mathbf{Q}_t)$
	$\mathbf{Q}_t$	The QSI at time slot t, $\mathbf{Q}_t := \{Q_{i,t}^{(c)} \vert q_i^{(c)} \in \Theta\}$
	$\mathbf{H}_t$	The CSI at time slot t, $\mathbf{H}_t := \{\mathbf{H}_{ij,t} \vert (i,j) \in \widetilde{\mathcal{L}}\}$
	$\mathbf{H}_{ij,t}$	The CSI of link (i,j) at time slot t
	$\mathbf{S}_{i,t}^{(c)}$	The local system state for SQM (i,c) at time slot t
Probability	$\mathbf{P}^{\Omega}$	The global state transition probability matrix under scheduling policy Ω
	$\boldsymbol{\pi}^{\Omega}$	The global steady-state probability matrix under scheduling policy Ω
	$\mathbf{P}_{(i,c)}^{\Omega}$	The local state transition probability matrix for SQM (i,c) under scheduling policy Ω
	$\boldsymbol{\pi}_{(i,c)}^{\Omega}$	The local steady-state probability matrix for SQM (i,c) under scheduling policy Ω
Performance Metrics	$\overline{Q}_i^{(c)}$	The average queue length of queue $q_i^{(c)}$
	$\overline{T}_c$	The mean throughput of connection c
	$\overline{D}_c$	The average packet delay of connection c
	d_c	The packet dropping probability of connection c

C_{d} downlink CUEs (with $N = 2D + C_{\mathrm{u}} + C_{\mathrm{d}}$). For example, in Fig. 1, we have $\mathcal{N}_{\mathrm{D}} = \{1,2\}$, $\mathcal{N}_{\mathrm{Cu}} = \{3\}$, and $\mathcal{N}_{\mathrm{Cd}} = \{4\}$.

Each transmission link represents a communication channel for direct transmission from a given node i to another node j, and is labeled by (i,j) (where $i,j \in \mathcal{N}$). Note that link (i,j) is distinct from link (j,i). The link set $\mathcal{L}$ is composed of three non-overlapping subsets, where $\mathcal{L}_{\mathrm{D}} := \{(i,i+1) \vert i \in \mathcal{N}_{\mathrm{Ds}}\}$ is the set of D2D links, $\mathcal{L}_{\mathrm{Cu}} := \{(i,0) \vert i \in \mathcal{N}_{\mathrm{Cu}} \bigcup \mathcal{N}_{\mathrm{Ds}}\}$ is the set of cellular uplinks, and $\mathcal{L}_{\mathrm{Cd}} := \{(0,i) \vert i \in \mathcal{N}_{\mathrm{Cd}} \bigcup \mathcal{N}_{\mathrm{Dd}}\}$ is the set of cellular downlinks. For example, in Fig. 1, we have $\mathcal{L}_{\mathrm{D}} = \{(1,2)\}$, $\mathcal{L}_{\mathrm{Cu}} = \{(3,0),(1,0)\}$, and $\mathcal{L}_{\mathrm{Cd}} = \{(0,4),(0,2)\}$.

All data that enter the network are associated with a particular connection $c \in \mathcal{C}$, which defines the source and destination of the data. Let $\mathcal{C}_{\mathrm{D}} = \{1, \ldots, D\}$ represent the set of

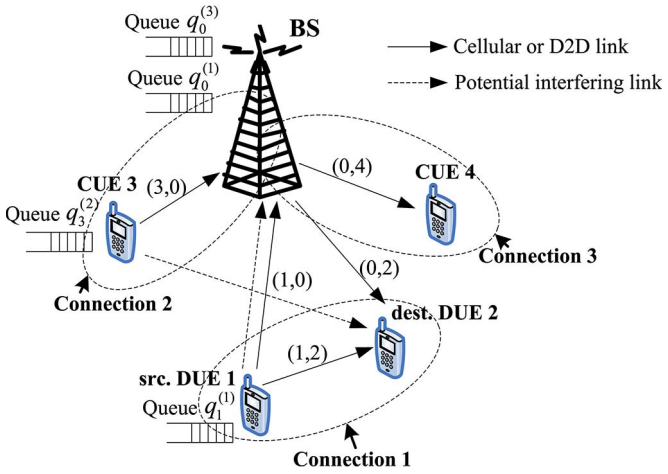

Fig. 1. Cellular networks with D2D communications capability.

D D2D connections, $\mathcal{C}_{\rm Cu} = \{D+1, \ldots, D+C_{\rm u}\}$ represent the set of $C_{\rm u}$ cellular uplink connections, and $\mathcal{C}_{\rm Cd} = \{D+C_{\rm u}+1, \ldots, D+C_{\rm u}+C_{\rm d}\}$ represent the set of $C_{\rm d}$ cellular downlink connections. Therefore, we have $\mathcal{C} := \{1, \ldots, C\} = \mathcal{C}_{\rm D} \bigcup \mathcal{C}_{\rm Cu} \bigcup \mathcal{C}_{\rm Cd}$ (with $C = D + C_{\rm u} + C_{\rm d}$). For example, in Fig. 1, there are $C = 3$ connections, with $\mathcal{C}_{\rm D} = \{1\}$, $\mathcal{C}_{\rm Cu} = \{2\}$, and $\mathcal{C}_{\rm Cd} = \{3\}$.

B. Routing Mode and Link Constraint Set

Define $\mathcal{L}_c$ as the set of all links (i,j) that connection c data is allowed to use. Obviously, $\mathcal{L}_c = \{(D+c, 0)\}$ for any cellular uplink connections $c \in \mathcal{C}_{\rm Cu}$, and $\mathcal{L}_c = \{(0, D+c)\}$ for any cellular downlink connections $c \in \mathcal{C}_{\rm Cd}$, since there is only a single-hop route between the CUE and the BS for these connections. For example, in Fig. 1, we have $\mathcal{L}_2 = \{(3,0)\}$ and $\mathcal{L}_3 = \{(0,4)\}$. However, the link constraint set $\mathcal{L}_c$ for any D2D connection $c \in \mathcal{C}_{\rm D}$ depends on which of the following Routing Modes (RMs) is chosen, i.e., whether the single hop route of D2D link or the two-hop route of cellular links can be used:

1) **D2D RM**, i.e., the connection c data is always transmitted via the D2D link, i.e., $\mathcal{L}_c = \{(2c-1, 2c)\}$;
2) **Cellular RM**, i.e., the connection c data is always transmitted via cellular links, i.e., $\mathcal{L}_c = \{(2c-1, 0), (0, 2c)\}$;
3) **Hybrid Mode**, i.e., the packets for connection c can be transmitted either via the D2D or cellular links, and the decision is made dynamically at each time slot, i.e., $\mathcal{L}_c = \{(2c-1, 2c), (2c-1, 0), (0, 2c)\}$.

For example, in Fig. 1, $\mathcal{L}_1$ equals {(1, 2)} in D2D RM, {(1, 0), (0, 2)} in Cellular RM, and {(1, 2), (1, 0), (0, 2)} in Hybrid RM. Let $\mathcal{C}_{\rm D1}$ and $\mathcal{C}_{\rm D2}$, and $\mathcal{C}_{\rm D3}$ represent the set of D2D connections in D2D RM, Cellular RM, and Hybrid RM, respectively.

When the RM and link constraint set $\mathcal{L}_c$ are determined for every D2D connection $c \in \mathcal{C}_{\rm D}$, the set of eligible links in the network $\widetilde{\mathcal{L}} := \sum_{c \in \mathcal{C}} \mathcal{L}_c$ is a subset of $\mathcal{L}$. This is because the corresponding D2D link (resp. cellular links) does not exist for a D2D connection in Cellular RM (resp. D2D RM). Therefore, $\widetilde{\mathcal{L}} = \widetilde{\mathcal{L}}_{\rm D} \bigcup \widetilde{\mathcal{L}}_{\rm Cu} \bigcup \widetilde{\mathcal{L}}_{\rm Cd}$, where $\widetilde{\mathcal{L}}_* = \sum_{c \in \mathcal{C}_*} \mathcal{L}_c$ and $*$ is a wildcard representing any of the characters in the set $\{{\rm D}, {\rm Cu}, {\rm Cd}\}$. Let $L := |\widetilde{\mathcal{L}}|$ denote the total number of links. Since $|\mathcal{L}_c|$ equals 1, 2, or 3 when connection c belongs to $\mathcal{C}_{\rm D1}$, $\mathcal{C}_{\rm D2}$, or $\mathcal{C}_{\rm D3}$, respectively, we have $L = C_{\rm u} + C_{\rm d} + D_1 + 2D_2 + 3D_3$, where D_1, D_2, and D_3 denote the number of D2D connections in the three RMs, respectively.

C. Scheduling and Resource Reuse Group

We consider slot-by-slot transmissions and each time slot has an equal length ΔT. There is an uplink scheduler and a downlink scheduler in the BS, which make independent scheduling decisions. The scheduling decision is responsible for selecting the set of links for uplink or downlink data transmissions at the beginning of each time slot $t \in \{0, 1, \ldots\}$. We assume that the D2D links $(i,j) \in \widetilde{\mathcal{L}}_{\rm D}$ can only use the cellular uplink resources, which is easier to implement from the protocol design perspective [1]. As discussed in the Introduction, we consider interference scenario (2) in this paper, i.e., the interference between a cellular user and a D2D user. Therefore, we assume a D2D link in the NOS resource sharing mode can reuse radio resources with a fixed cellular uplink, while a D2D link uses orthogonal resources with cellular uplinks in the OS resource sharing mode.

We define a Resource Reuse Group (RRG) $\mathcal{B}_u$ as the subset of links $(i,j) \in \widetilde{\mathcal{L}}$ that can be scheduled for uplink or downlink transmission simultaneously in a time slot. Therefore, a RRG for uplink transmission may contain at most one cellular uplink and one D2D link. On the other hand, a RRG for downlink transmission can contain one and only one cellular downlink. Let $\mathcal{U}$ represent the set of RRG indexes, $\mathcal{U}_{\rm u}$ and $\mathcal{U}_{\rm d}$ represent the subsets of RRG indexes for uplink and downlink transmissions, respectively. Therefore, we have $\mathcal{U} = (\mathcal{U}_{\rm u}, \mathcal{U}_{\rm d})$. For any link $(i,j) \in \widetilde{\mathcal{L}}$, define $\mathcal{U}_{ij} := \{u | (i,j) \in \mathcal{B}_u, u \in \mathcal{U}\}$ as the index set of RRGs that contain link (i,j). For example, in Fig. 1, when connection 1 works in the Hybrid RM with no resource allocation restrictions, there are four RRGs in the uplink, and we let $\mathcal{B}_1 = \{(1,2)\}$, $\mathcal{B}_2 = \{(3,0)\}$, $\mathcal{B}_3 = \{(1,2), (3,0)\}$, and $\mathcal{B}_4 = \{(1,0)\}$. Moreover, there are two RRGs in the downlink, and we let $\mathcal{B}_5 = \{(0,4)\}$, $\mathcal{B}_6 = \{(0,1)\}$. Therefore, we have $\mathcal{U} = \{1,2,3,4,5,6\}$, $\mathcal{U}_{\rm u} = \{1,2,3,4\}$, $\mathcal{U}_{\rm d} = \{5,6\}$, $\mathcal{U}_{12} = \{1,3\}$, $\mathcal{U}_{30} = \{2,3\}$, $\mathcal{U}_{10} = \{4\}$, $\mathcal{U}_{04} = \{5\}$, and $\mathcal{U}_{01} = \{6\}$. In each time slot, at most one RRG can be scheduled for uplink or downlink transmissions. Let $x_{u,t} \in \{0,1\}$ denote the scheduling result for RRG $\mathcal{B}_u$, $u \in \mathcal{U}$ at time slot t, where $x_{u,t} = 1$ if RRG $\mathcal{B}_u$ is scheduled, and $x_{u,t} = 0$ otherwise.

D. Communications Mode

The three RMs can be combined with different resource allocation restrictions to result in seven Communications Modes, which can model the semi-static or dynamic selection of the three RSMs in [9], i.e., NOS, OS and CM. This is illustrated in Table II taking the simple network in Fig. 1 as an example. In the D2D RM, we can model the semi-static selection of OS or NOS RSM if we restrict the uplink scheduler to choose only from RRGs $\mathcal{B}_1$ and $\mathcal{B}_2$ or choose only RRG $\mathcal{B}_3$ in each time slot. We refer to the former as D2D-NOS Mode, while the latter as

TABLE II
RELATIONSHIPS BETWEEN THE ROUTING MODES, COMMUNICATIONS MODES AND THE SEMI-STATIC OR DYNAMIC SELECTIONS OF THE RESOURCE SHARING MODES

Routing Mode	Communications Mode	Resource Allocation Restriction	(Semi-)Static or Dynamic Selection of the Three Resource Sharing Modes
D2D RM	D2D-OS Mode	$\mathcal{B}_1$, $\mathcal{B}_2$	**semi-static** selection of OS RSM
	D2D-NOS Mode	$\mathcal{B}_3$	**semi-static** selection of NOS RSM
	D2D-dynamic Mode	$\mathcal{B}_1$, $\mathcal{B}_2$, $\mathcal{B}_3$	**dynamic** selection between OS and NOS RSMs
Cellular RM	Cellular Mode	$\mathcal{B}_2$, $\mathcal{B}_4$	**semi-static** selection of CM RSM
Hybrid RM	Hybrid-OS Mode	$\mathcal{B}_1$, $\mathcal{B}_2$, $\mathcal{B}_4$	**dynamic** selection between OS and CM RSMs
	Hybrid-NOS Mode	$\mathcal{B}_3$, $\mathcal{B}_4$	**dynamic** selection between NOS and CM RSMs
	Hybrid-Dynamic Mode	$\mathcal{B}_1$, $\mathcal{B}_2$, $\mathcal{B}_3$, $\mathcal{B}_4$	**dynamic** selection between OS, NOS, CM RSMs

D2D-OS Mode. On the other hand, the D2D RM can model the dynamic selection between the NOS and OS RSMs if the uplink scheduler is allowed to choose from all of RRGs $\mathcal{B}_1$, $\mathcal{B}_2$, and $\mathcal{B}_3$, which is referred to as D2D-Dynamic Mode. We will refer to the D2D-Dynamic Mode when D2D Mode is mentioned in the rest of this paper without explicit explanation. The Cellular RM (Cellular Mode) models the semi-static selection of the CM RSM. The Hybrid RM models the dynamic selection of all the three RSMs (Hybrid-Dynamic Mode) when it can choose from all of the RRGs $\mathcal{B}_1$, $\mathcal{B}_2$, $\mathcal{B}_3$, and $\mathcal{B}_4$, while it models the dynamic selection between NOS and CM (Hybrid-NOS Mode) or OS and CM (Hybrid-OS Mode) with the corresponding resource allocation restriction. We will implicitly refer to Hybrid-Dynamic Mode in the following discussion on the Hybrid Mode.

In our paper, mode selection refers to the selection of a Communications Mode instead of a RSM in [9]. When a pair of D2D UEs wants to setup a connection, it first chooses a communications mode. When the D2D-NOS, D2D-OS, or Cellular Mode is chosen, the RSM is also determined and the uplink scheduler only performs resource allocation. On the other hand, if the D2D-Dynamic Mode or any of the three Hybrid Modes is chosen, the uplink scheduler performs both dynamic RSM selection and resource allocation. Moreover, a cellular uplink $(i_c, 0)$ is determined by the D2D connection c with whom it can form a RRG if D2D-NOS, D2D-Dynamic, Hybrid-NOS or Hybrid-Dynamic Mode is chosen. The application of the queuing model and numerical evaluation method proposed in this paper to the mode selection scheme under non-saturated traffic model is discussed in Section V.

E. Queuing Dynamics

Let $A_{c,t}$ denote the amount of new connection c data[1] that exogenously arrives to its source node during time slot t. We assume that the data arrival process is i.i.d. over time slots following general distribution with average arrival rate $\mathbf{E}[A_{c,t}] = \lambda_c$, where $\Pr.(A_c = arr) > 0$ if $arr \geq 0$. The data is transmitted hop by hop along the route(s) of the connection to its destination node. Each node i along the route(s) of connection c maintains a queue $q_i^{(c)}$ for storing its data except for the destination node, since the data is assumed to exit the network once it reaches the destination. We assume each queue has a finite capacity of $N_{\mathrm{Q}} < \infty$ (in number of bits or packets). Define Θ as the set of queues in the system. For example, in Fig. 1, we have four queues if Cellular RM or Hybrid RM is chosen for D2D connection 1, i.e., $\Theta = \{q_1^{(1)}, q_0^{(1)}, q_3^{(2)}, q_0^{(3)}\}$. On the other hand, if D2D RM is chosen for D2D connection 1, there are only three queues, i.e., $\Theta = \{q_1^{(1)}, q_3^{(2)}, q_0^{(3)}\}$. Let $Q_{i,t}^{(c)}$ denote the length of $q_i^{(c)}$ at the beginning of time slot t.

We assume that a RRG is scheduled for transmission only when all its links have non-empty queues. A queue $q_i^{(c)}$ is scheduled in time slot t when at least one RRG $\mathcal{B}_u$ containing a link $(i,j) \in \mathcal{L}_c$ is scheduled. Only when a queue is scheduled shall it move the data out of the queue for transmission. We consider the transmission capability for queue $q_i^{(c)}$ during time slot t as $r_{i,t}^{(c)}$, where $r_{i,t}^{(c)}$ is the instantaneous data rate[2] of queue $q_i^{(c)}$ during time slot t. $r_{i,t}^{(c)}$ is equal to the sum of the instantaneous data rate of the scheduled link $(i,j) \in \mathcal{L}_c$ at time slot t, i.e.,

$$r_{i,t}^{(c)} = \sum_{(i,j)\in\mathcal{L}_c} r_{ij,t}, \tag{1}$$

where

$$r_{ij,t} = \sum_{u\in\mathcal{U}_{ij}} x_{u,t} r_{ij,t}^{(u)}, \tag{2}$$

and $r_{ij,t}^{(u)}$ is the instantaneous data rate of link (i,j) when RRG $\mathcal{B}_u$ is scheduled, since different amount of interference for link (i,j) will arise when different RRGs are scheduled. Therefore, $r_{ij,t} = r_{ij,t}^{(u)}$ if RRG $\mathcal{B}_u$ containing link (i,j) is scheduled, and $r_{ij,t} = 0$ if none of the RRGs containing link (i,j) is scheduled.

If the value of $Q_{i,t}^{(c)}$ is less than the value of $r_{i,t}^{(c)}$ during time slot t, padding bits shall be transmitted along with the data. Arriving data is placed in the queue throughout the time slot t and can only be transmitted during the next time slot $t+1$. If the queue length reached the buffer capacity N_{Q}, the subsequent arriving data will be dropped. Let $A_{i,t}^{(c)}$ denote the units of data arrived to node i for connection c during the time slot t. If node i is the source node of connection c, then $A_{i,t}^{(c)} = A_{c,t}$. This applies to the scenario when connection c

[1]The data can take units of bits or packets. The latter is appropriate when all the packets have fixed length.

[2]The instantaneous data rate can take units of bits/slot or packets/slot. The latter is appropriate when all the packets have fixed length and the achievable data rates are constrained to integral multiples of the packet size.

is a cellular connection or a D2D connection in D2D RM, i.e., $c \in \mathcal{C}_{\mathrm{Cu}} \bigcup \mathcal{C}_{\mathrm{Cd}} \bigcup \mathcal{C}_{\mathrm{D1}}$. Moreover, if connection c is a D2D connection in Cellular RM or Hybrid RM, this also applies when node i is the src. DUE, i.e., $c \in \mathcal{C}_{\mathrm{D2}} \bigcup \mathcal{C}_{\mathrm{D3}}$ and $i \in \mathcal{N}_{\mathrm{Ds}}$. Otherwise, $A_{i,t}^{(c)}$ depends on the data departure process of the corresponding uplink transmission. This applies when connection c is a D2D connection in Cellular RM or Hybrid RM and node i is the BS, i.e., $c \in \mathcal{C}_{\mathrm{D2}} \bigcup \mathcal{C}_{\mathrm{D3}}$ and $i = 0$. According to the above assumption, the queuing process evolves as follows:

$$Q_{i,t+1}^{(c)} = \min\left[N_{\mathrm{Q}}, \max\left[0, Q_{i,t}^{(c)} - r_{i,t}^{(c)}\right] + A_{i,t}^{(c)}\right]. \quad (3)$$

F. Instantaneous Data Rate

The instantaneous data rate $r_{i,t}^{(c)}$ of $q_i^{(c)}$ is dependent on the instantaneous data rate $r_{ij,t}^{(u)}$ of link $(i,j) \in \mathcal{L}_c$ when RRG $\mathcal{B}_u, u \in \mathcal{U}_{ij}$ is scheduled according to (1) and (2). Therefore, it is essential to determine the value of $r_{ij,t}^{(u)}$.

For any link $(i,j) \in \widetilde{\mathcal{L}}_{\mathrm{D}} \bigcup \widetilde{\mathcal{L}}_{\mathrm{Cu}}$, we define its potential interfering link as the communication channel from the transmitter of any link that belongs to the same RRG with link (i,j) to the receiver of node j. Define $\mathcal{I}_{ij} := \{I_{i'j} | (i',j') \in \mathcal{B}_u \setminus \{i,j\}, u \in \mathcal{U}_{ij}\}$ as the set of potential interfering links of link (i,j), where $I_{i'j}$ denotes the potential interfering link from the transmitter of node i' to the receiver of node j. For example, in Fig. 1, we have $\mathcal{I}_{30} = \{I_{10}\}$ and $\mathcal{I}_{12} = \{I_{32}\}$, since cellular uplink (3, 0) and D2D link (1, 2) can reuse the same radio resources. An interfering link is 'potential' since it only exists when the corresponding RRG is scheduled for transmission. Since there are two categories of links, i.e., transmission links and potential interfering links, all links mentioned are referred to the transmission links by default in the rest of the paper.

Assume that the instantaneous channel gain comprising the path loss, shadowing and fast fading effects of the wireless channel from the transmitter of node $i \in \mathcal{N}$ to the receiver of node $j \in \mathcal{N}$ remains constant within a time slot, the value of which at time slot t is denoted by $G_{ij,t}$. Let $p_{ij,t}$ be the transmission power of link $(i,j) \in \mathcal{L}$ at time slot t. Let $\gamma_{ij,t} := (p_{ij,t} G_{ij,t})/N_{ij}$ represent the Signal to Noise Ratio (SNR) of link $(i,j) \in \widetilde{\mathcal{L}}$, where N_{ij} is the noise power. The SINR value of a link (i,j) may or may not equal its SNR value, depending on whether there are any other links that are scheduled simultaneously with link (i,j) and thus causing interference to each other. Specifically, assume that RRG $\mathcal{B}_u$ is scheduled at time slot t, we have

$$SINR_{ij,t}^{(u)} = \frac{p_{ij,t} G_{ij,t}}{N_{ij,t} + \sum_{(i',j') \in \mathcal{B}_u \setminus \{(i,j)\}} p_{i'j',t} G_{i'j,t}} = \frac{\gamma_{ij,t}}{1 + \sum_{(i',j') \in \mathcal{B}_u \setminus \{(i,j)\}} \gamma_{i'j,t}}, \ \forall (i,j) \in \mathcal{B}_u. \quad (4)$$

The corresponding instantaneous data rate $r_{ij,t}^{(u)}$ is a function of $SINR_{ij,t}^{(u)}$. We assume that Adaptive Modulation and Coding (AMC) is used, where the SINR values are divided into K non-overlapping consecutive regions. For any $k \in \{1, \ldots, K\}$, if the SINR value $SINR_{ij,t}^{(u)}$ of link (i,j) falls within the k-th region $[\Gamma_{k-1}, \Gamma_k)$, the corresponding data rate $r_{ij,t}^{(u)}$ of link (i,j) is a fixed value R_k according to the selected modulation and coding scheme in this state, i.e., $r_{ij,t}^{(u)} = R_k$, if $SINR_{ij,t}^{(u)} \in [\Gamma_{k-1}, \Gamma_k)$. Obviously, $\Gamma_0 = 0$ and $\Gamma_K = \infty$. Also, we have $R_1 = 0$, i.e., no packet is transmitted in channel state 1 to avoid the high transmission error probability.

III. Queuing Model

A. Model Description

The queuing model (QM) for the above general network model is illustrated in Fig. 2. With a slight abuse of notation, we also use (i,j) to denote the server in the QM corresponding to link (i,j). We use a black and a white circle to illustrate a server corresponding to a cellular link and a D2D link, respectively.

As the set of connections can be divided into five non-overlapping subsets, i.e., $\mathcal{C}_{\mathrm{D1}}$, $\mathcal{C}_{\mathrm{D2}}$, $\mathcal{C}_{\mathrm{D3}}$, $\mathcal{C}_{\mathrm{Cu}}$, and $\mathcal{C}_{\mathrm{Cd}}$, the queues and servers in the general QM can also be divided accordingly. For any cellular uplink or downlink connection, or D2D connection in D2D RM, i.e., $c \in \mathcal{C}_{\mathrm{Cu}} \bigcup \mathcal{C}_{\mathrm{Cd}} \bigcup \mathcal{C}_{\mathrm{D1}}$, since there is only one single-hop route, its QM has a single queue with a data arrival process of mean λ_c, and a single server. For any D2D connection $c \in \mathcal{C}_{\mathrm{D2}}$ in Cellular RM, since there is one two-hop route, the connection can be formulated as a two-stage tandem queuing model. Specifically, there is a queue $q_{2c-1}^{(c)}$ having a stage-1 server corresponding to link $(2c-1, 0)$ and a queue $q_0^{(c)}$ having a stage-2 server corresponding to link $(0, 2c)$. The data arrives with mean λ_c at the queue $q_{2c-1}^{(c)}$, and joins $q_0^{(2c)}$ immediately after it receives service from the stage-1 server, and upon completion of service at the stage-2 server leaves the system. For any D2D connection $c \in \mathcal{C}_{\mathrm{D3}}$ in Hybrid RM, since the data can be either transmitted via the one-hop route or two-hop route, the connection can be formulated as a two-stage tandem queuing model as well. The only difference from the tandem queuing model of the Cellular RM is that there are two stage-1 servers for queue $q_{2c-1}^{(c)}$, corresponding to link $(2c-1, 2c)$ and link $(2c-1, 0)$, respectively. The data in $q_{2c-1}^{(c)}$ served by server $(2c-1, 0)$ will join $q_0^{(c)}$ immediately after it receives service from the stage-1 server, and upon completion of service at the stage-2 server left the system. On the other hand, the data in $q_{2c-1}^{(c)}$ served by server $(2c-1, 2c)$ will leave the system directly upon completion.

B. System State

The global system state of the above QM at time slot t can be characterized by the aggregation of the CSI and QSI, i.e., $\mathbf{S}_t = (\mathbf{H}_t, \mathbf{Q}_t)$. Let $\mathcal{S} = \mathcal{H} \times \mathcal{Q}$ be the full system state space. The QSI is defined as $\mathbf{Q}_t := \{Q_{i,t}^{(c)} | q_i^{(c)} \in \Theta\}$, which is a vector consisting of the lengths of all the queues at the beginning of time slot t. The CSI is defined as $\mathbf{H}_t := \{\mathbf{H}_{ij,t} | (i,j) \in \widetilde{\mathcal{L}}\}$, where $\mathbf{H}_{ij,t}$ denotes the CSI of link (i,j) in time slot t. We refer to the aggregate CSI for all the cellular uplinks and D2D links as uplink CSI, which is denoted as

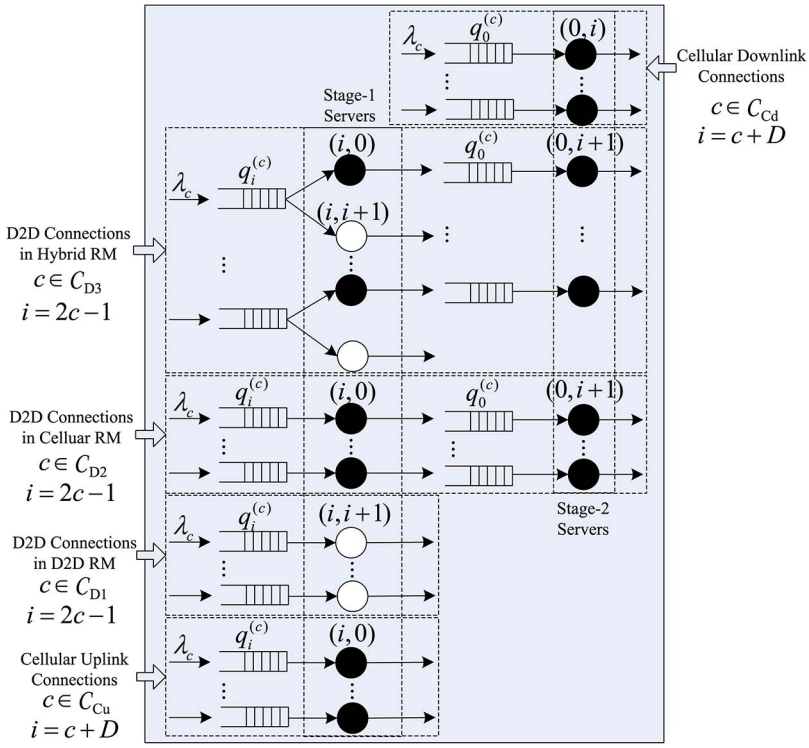

Fig. 2. Queuing model for the general network model.

$\mathbf{H}_{\mathrm{u},t} := \{\mathbf{H}_{ij,t} | (i,j) \in \widetilde{\mathcal{L}}_{\mathrm{Cu}} \bigcup \widetilde{\mathcal{L}}_{\mathrm{D}}\}$. Similarly, the downlink CSI is defined as $\mathbf{H}_{\mathrm{d},t} := \{\mathbf{H}_{ij,t} | (i,j) \in \widetilde{\mathcal{L}}_{\mathrm{Cd}}\}$, which is the aggregate CSI for all the cellular downlinks. Therefore, we have $\mathbf{H}_t = (\mathbf{H}_{\mathrm{u},t}, \mathbf{H}_{\mathrm{d},t})$. We will discuss the definition of $\mathbf{H}_{ij,t}$ for uplink CSI and downlink CSI, respectively.

It is much easier to represent the downlink CSI than the uplink CSI, since there is no interference between the cellular downlinks. Assume that every scheduled link always transmits at constant power $P_{\max}$, where $P_{\max}$ is the maximum transmit power of a node. We consider a narrowband downlink of flat fading channel. A Rayleigh or Nakagami-m fading channel can be approximated by a finite state Markov model, which is widely acknowledged as a reasonably accurate and mathematically tractable approach. With this approach, the channel of any cellular downlink is in state k if its received SNR is between $[\Gamma_{k-1}, \Gamma_k)$, where the SNR threshold Γ_k, $k \in \{1, \ldots, K\}$ is defined by the AMC scheme. Therefore, the downlink CSI per link can be represented by $\mathbf{H}_{ij,t} = H_{ij,t}$, $\forall\, (i,j) \in \widetilde{\mathcal{L}}_{\mathrm{Cd}}$, where $H_{ij,t} \in \{1, \ldots, K\}$ denotes the channel state of link $(i,j) \in \widetilde{\mathcal{L}}_{\mathrm{Cd}}$.

The representation of the uplink CSI for the general network model is more complex. When every scheduled link transmits at constant power $P_{\max}$, we can define $\mathbf{H}_{ij,t} := \{H_{ij,t}^{(u)} | u \in \mathcal{U}_{ij}\}$, $\forall (i,j) \in \widetilde{\mathcal{L}}_{\mathrm{Cu}} \bigcup \widetilde{\mathcal{L}}_{\mathrm{D}}$, where $H_{ij,t}^{(u)}$ denotes the channel state of link (i,j) when RRG $\mathcal{B}_u$ is scheduled. Specifically, $H_{ij,t}^{(u)} = k$ if $SINR_{ij,t}^{(u)}$ is between $[\Gamma_{k-1}, \Gamma_k)$. Although the local CSI space size for any link $(i,j) \in \widetilde{\mathcal{L}}_{\mathrm{Cu}} \bigcup \widetilde{\mathcal{L}}_{\mathrm{D}}$ grows exponentially with the number of RRGs that it belongs to, i.e., $|\mathcal{U}_{ij}|$, we have $|\mathcal{U}_{ij}| \leq 2$ due to our assumption on resource sharing restriction that a cellular uplink can only reuse radio resources with at most one D2D link.

C. Resource Reuse Group (RRG) Scheduling Policy

In each time slot, the BS observes the system state $\mathbf{S}_t$ and chooses a RRG scheduling action $\mathbf{a}$ from the set of allowable actions in the action space $\mathcal{A}$. An action $\mathbf{a}$ is composed of an uplink scheduling action $\mathbf{a}_{\mathrm{u}} \in \mathcal{A}_{\mathrm{u}}$ and a downlink scheduling action $\mathbf{a}_{\mathrm{d}} \in \mathcal{A}_{\mathrm{d}}$, i.e., $\mathbf{a} := (\mathbf{a}_{\mathrm{u}}, \mathbf{a}_{\mathrm{d}})$, where $\mathbf{a}_* := \{x_u \in \{0,1\} | u \in \mathcal{U}_*\} \in \mathcal{A}_*$. Without explicit explanation, let $*$ be a wildcard representing any of the characters in the set $\{\mathrm{u}, \mathrm{d}\}$ in the rest of the paper. Since at most one RRG $\mathcal{B}_u$ can be scheduled for any uplink or downlink scheduling action $\mathbf{a}_*$, there are $|\mathcal{U}_*| + 1$ actions in the set $\mathcal{A}_*$. Denote $\mathbf{a}_*^{(u)}$, $u \in \{0\} \bigcup \mathcal{U}_*$ as an action in $\mathcal{A}_*$, where $\mathbf{a}_*^{(0)} = \mathbf{0}$ means that no RRG is scheduled and $\mathbf{a}_*^{(u)}$, $u \neq 0$ means that RRG $\mathcal{B}_u$ is scheduled.

A control policy prescribes a procedure for action selection in each state at all decision epoches t. We consider stationary Markovian randomized control policies. Specifically, a RRG scheduling policy consists of an uplink policy $\Omega_{\mathrm{u}}(\mathbf{S})$ and a downlink policy $\Omega_{\mathrm{d}}(\mathbf{S})$, where $\Omega_*(\mathbf{S}) = \{\phi_{\mathbf{S}}(\mathbf{a}_*) | \mathbf{a}_* \in \mathcal{A}_*\}$, $\forall\, \mathbf{S} \in \mathcal{S}$ is a mapping $\mathcal{S} \to \mathcal{P}(\mathcal{A}_*)$ from the state space to the set of probability distributions on the action space. Therefore, $\phi_{\mathbf{S}}(\mathbf{a}_*^{(u)})$, $u \in \mathcal{U}_*$, corresponds to the selection probability of RRG $\mathcal{B}_u$ under the given uplink or downlink RRG scheduling policy.

Many existing channel-aware and/or queue-aware scheduling algorithms for wireless networks usually select the user with the largest utility, which is a function of the CSI and/or QSI. Examples include MaxWeight, Exponential (Exp) rule, and Log rule scheduling algorithms. Since more than one user with the largest utility may exist, one of these eligible users can be randomly selected, and this category of control policies become

randomized. Assume that the uplink and downlink scheduling policies are all set to the MaxWeight scheduler, which observes the queue and channel states $(\mathbf{H}_t, \mathbf{Q}_t)$ of the system at every time slot t. For each link $(i,j) \in \widetilde{\mathcal{L}}$, define its weight as the maximum value of 0 and its differential backlog

$$W_{ij}(\mathbf{Q}_t) = \max\left[Q_{i,t}^{(c)} - Q_{j,t}^{(c)}, 0\right], \text{ s.t. } (i,j) \in \mathcal{L}_c. \quad (5)$$

Note that for any link $(i,j) \in \widetilde{\mathcal{L}}$ which belongs to a single-hop route or is the second hop of a two-hop route, the queue $q_j^{(c)}$ doesn't exist and we have $Q_{j,t}^{(c)} = 0$.

For the MaxWeight algorithm, the RRG with maximum sum over all its links of the product of link weight and link transmission rate is served. Therefore, the selection probability $\phi_{\mathbf{S}}(\mathbf{a}_*^{(u)})$ can be found as

$$\phi_{\mathbf{S}}\left(\mathbf{a}_*^{(u)}\right) = \begin{cases} 1/\left\|\mathrm{MAW}(\mathbf{S})\right\|, & \text{if } u \in \mathrm{MAW}(\mathbf{S}) \\ 0, & \text{otherwise,} \end{cases} \quad (6)$$

where $\mathrm{MAW}(\mathbf{S}) = \{u \mid \sum_{(i,j)\in\mathcal{B}_u} W_{ij}(\mathbf{Q}) R_{H_{ij}^u} = \max_{v\in\mathcal{U}_*} (\sum_{(i',j')\in\mathcal{B}_v} W_{i'j'}(\mathbf{Q}) R_{H_{i'j'}^v}),\ \prod_{(i,j)\in\mathcal{B}_u} Q_i^{(c)} > 0, u \in \mathcal{U}_*\}$.

It is proven in [16] that the MaxWeight algorithm can guarantee queue stability under a general topology including both cellular and wireless multi-hop networks, since it gives priority to a queue when it starts to get too large. Other RRG scheduling policies can be represented in a similar way.

IV. Performance Analysis

A. Exact Solution of Steady-State Probabilities

The system behavior of the above QM can be represented by the DTMC $\{\mathbf{S}_t\}_{t=0,1,\ldots} := \{(\mathbf{H}_t, \mathbf{Q}_t)\}_{t=0,1,\ldots}$. Given a system state $\mathbf{S}_t$ and a scheduling action $\mathbf{a}$ at time slot t, the state transition probability of the DTMC is given by:

$$\begin{aligned} &\Pr\left\{\mathbf{S}_{(t+1)} | \mathbf{S}_t, \mathbf{a}\right\} \\ &= \Pr\left\{\mathbf{H}_{(t+1)} | \mathbf{S}_t, \mathbf{a}\right\} \Pr\left\{\mathbf{Q}_{(t+1)} | \mathbf{S}_t, \mathbf{a}\right\} \\ &= \Pr\left\{\mathbf{H}_{\mathrm{d},(t+1)} | \mathbf{H}_{\mathrm{d},t}\right\} \Pr\left\{\mathbf{H}_{\mathrm{u},(t+1)} | \mathbf{H}_{\mathrm{u},t}\right\} \Pr\left\{\mathbf{Q}_{(t+1)} | \mathbf{S}_t, \mathbf{a}\right\} \\ &= p_{\mathbf{H}_{\mathrm{d},t}}^{\mathbf{H}_{\mathrm{d},(t+1)}} p_{\mathbf{H}_{\mathrm{u},t}}^{\mathbf{H}_{\mathrm{u},(t+1)}} p_{(\mathbf{S}_t,\mathbf{a})}^{\mathbf{Q}_{(t+1)}}. \end{aligned} \quad (7)$$

The first two elements, i.e., $p_{\mathbf{H}_{\mathrm{d},t}}^{\mathbf{H}_{\mathrm{d},(t+1)}}$ and $p_{\mathbf{H}_{\mathrm{u},t}}^{\mathbf{H}_{\mathrm{u},(t+1)}}$, represent the downlink and uplink CSI transition probabilities, respectively, which are independent of the scheduling action $\mathbf{a}$. The third element, i.e., $p_{(\mathbf{S}_t,\mathbf{a})}^{\mathbf{Q}_{(t+1)}}$, represents the QSI transition probability.

1) CSI Transition Probability: We assume that the instantaneous channel gains of the wireless channels between any pair of transmitters and receivers are independent from each other (e.g., the wide sense stationary uncorrelated scattering (WSSUS) model commonly used for the multipath fading channel [19]). Therefore, the (virtual) SNR $\gamma_{ij,t}$ for any transmission link or potential interfering link is statistically independent from that of the others. The downlink CSI transition probability $p_{\mathbf{H}_{\mathrm{d},t}}^{\mathbf{H}_{\mathrm{d},(t+1)}}$ can be derived as the product of local per-downlink CSI transition probabilities $p_{H_{ij,t}}^{H_{ij,(t+1)}}$ of every cellular downlink $(i,j) \in \widetilde{\mathcal{L}}_{\mathrm{Cd}}$, as there is no interference between the cellular downlinks so that the local per downlink CSIs $H_{ij,t}$ are stochastically independent from each other. The steady-state probability of local per downlink CSI $\lim_{t\to\infty} \Pr\{H_{ij,t} = k\}$ of each state k can be derived by integrating the pdf of the SNR over the corresponding region $[\Gamma_{k-1}, \Gamma_k)$. The state transition probability $p_{H_{ij,t}}^{H_{ij,(t+1)}}$ can be derived from integrating the joint pdf of the SNR over two consecutive time slots and over the desired regions defined by $H_{ij,t}$ and $H_{ij,(t+1)}$. When the rate of temporal channel variations is relatively slow and the number of states is not so high, the state transition probability can be approximated by level-crossing rate (LCR), which assumes that from time slot t to $t+1$, the CSI either stays in the same state or it transits to its immediate neighboring states [20].

The derivation of the uplink CSI transition probability $p_{\mathbf{H}_{\mathrm{u},t}}^{\mathbf{H}_{\mathrm{u},(t+1)}}$ is more complicated. First, the local per uplink CSI is a tuple $\mathbf{H}_{ij,t}$ which may consists of more than one elements. Since the elements $H_{ij,t}^{(u)}$, $u \in \mathcal{U}_{ij}$ within $\mathbf{H}_{ij,t}$ are correlated due to their common dependence on the SNR of link (i,j) from (4), the transition probability of local per uplink CSI $p_{\mathbf{H}_{ij,t}}^{\mathbf{H}_{ij,(t+1)}}$ cannot be further decomposed into the product of $p_{H_{ij,t}^{(u)}}^{H_{ij,(t+1)}^{(u)}}$. Second, when a D2D connection c works in the Hybrid Mode, the wireless channel from the transmitter of node $2c-1$ to the receiver of the BS is simultaneously a cellular uplink $(2c-1, 0)$ and a potential interfering link $I_{(2c-1)0}$ for another cellular uplink $(i_c, 0)$ which is assigned to reuse the radio resources with D2D link $(2c-1, 2c)$. Therefore, the local CSIs $H_{(2c-1)0,t}^{(u)}$ and $H_{i_c0,t}^{(v)}$ are correlated due to their common dependence on the (virtual) SNR $\gamma_{(2c-1)0,t}$ from (4). Due to the above two reasons, the uplink CSI transition probability $p_{\mathbf{H}_{\mathrm{u},t}}^{\mathbf{H}_{\mathrm{u},(t+1)}}$ cannot be completed decomposed into the product of the one-dimensional local CSI transition probabilities $p_{H_{ij,t}^{(u)}}^{H_{ij,(t+1)}^{(u)}}$. For example, in Fig. 1, it is obvious that $H_{12,t}^{(1)}$ and $H_{12,t}^{(3)}$ are correlated through $\gamma_{12,t}$ and $H_{30,t}^{(2)}$ and $H_{30,t}^{(3)}$ are correlated through $\gamma_{30,t}$. Moreover, as $SINR_{30,t}^{(3)}$ is dependent on $\gamma_{10,t}$, which is the virtual SNR of potential interfering link I_{10} and also the SNR of cellular uplink (1, 0), we have $H_{30,t}^{(3)}$ and $H_{10,t}^{(4)}$ are correlated through $\gamma_{10,t}$. For any other local CSI $H_{ij,t}^{(u)}$, we have $SINR_{ij,t}^{(u)} = \gamma_{ij,t}$, which means that it is independent from the other local CSIs due to the independence between SNRs. Therefore, when connection 1 works in different modes, $p_{\mathbf{H}_{\mathrm{u},t}}^{\mathbf{H}_{\mathrm{u},t+1}}$ can be decomposed as shown in (8) at the bottom of the next page.

Theoretically, the multi-dimensional local CSI transition probabilities $p_{(H_{12,t}^{(1)}, H_{12,t}^{(3)})}^{(H_{12,(t+1)}^{(1)}, H_{12,(t+1)}^{(3)})}$, $p_{(H_{30,t}^{(2)}, H_{30,t}^{(3)})}^{(H_{30,(t+1)}^{(2)}, H_{30,(t+1)}^{(3)})}$, and $p_{(H_{30,t}^{(2)}, H_{30,t}^{(3)}, H_{10,t}^{(4)})}^{(H_{30,(t+1)}^{(2)}, H_{30,(t+1)}^{(3)}, H_{10,(t+1)}^{(4)})}$ can also be derived from the integration method as the one-dimensional local CSI transition

probabilities. However, the computational complexity of the numerical evaluation of the double integration over the region defined by a two or three dimensional polyhedron forbids its practical application. Therefore, we use the Monte-Carlo method to obtain their transition probabilities. Since the Monte-Carlo simulation only depends on the statistical properties of the wireless channels and is irrelevant to the queuing dynamics, it only needs to be performed once for different traffic arrival rates or scheduling policies. Moreover, we only need to generate Rayleigh fading channels following the Jakes Model for the four wireless channels from any transmitter on nodes 1, 3 to any receiver on nodes 0, 2 in the Monte-Carlo simulation to obtain the above three transition probabilities simultaneously.

From the above discussion, we can see that the CSI state space $\mathcal{H}$ is the Cartesian product of the per link state space $\mathcal{H}_{ij}$, except the case when Hybrid Mode is chosen for a D2D connection c. In this case, the state space of the cellular uplink for D2D connection c, i.e., link $(2c-1,0)$, and the state space of the cellular uplink $(i_c,0)$ with resource reuse relationship with D2D link $(2c-1,2c)$ should be jointly considered. We denote this jointly considered state $\mathbf{H}_{i_c(2c-1)0}$ and state space as $\mathcal{H}_{i_c(2c-1)0}$. For example, in Fig. 1, the CSI state space of links (1, 0) and (3, 0) have to be jointly considered, i.e., $\mathbf{H}_{310} := (H_{30}^{(2)}, H_{30}^{(3)}, H_{10}^{(4)})$. Therefore, the CSI state space $\mathcal{H}$ grows exponentially with the number of links.

Theorem 1: The per link CSI state space $\mathcal{H}_{ij}$ and joint link CSI state space $H_{\widehat{(c+D)}(2c-1)0}$ are given as follows.

1) When $\mathcal{U}_{ij}=1$, we have $\mathbf{H}_{ij}=H_{ij}\in\{1,\ldots,K\}$. The cardinal of $\mathcal{H}_{ij}$ is K.
2) When $\mathcal{U}_{ij}=2$, we have $\mathbf{H}_{ij}=\{(H_{ij}^{(u1)},H_{ij}^{(u2)}):H_{ij}^{(u2)}\le H_{ij}^{(u1)}\in\{1,\ldots,K\}\}$. The cardinal of $\mathcal{H}_{ij}$ is $K(K+1)/2$.
3) For the joint link CSI state space $\mathcal{H}_{i_c(2c-1)0}$, we have $\mathbf{H}_{i_c(2c-1)0}=\{(H_{i_c0}^{(u1)},H_{i_c0}^{(u2)},H_{(2c-1)0}^{(u3)}):H_{i_c0}^{(u1)},H_{i_c0}^{(u2)},H_{(2c-1)0}^{(u3)}\in\{1,\ldots,K\},\Gamma_{(H_{i_c0}^{(u1)}-1)}\,/\,(\Gamma_{H_{(2c-1)0}^{(u3)}}+1)<\Gamma_{H_{i_c0}^{(u2)}}\le\Gamma_{H_{i_c0}^{(u1)}},\Gamma_{(H_{i_c0}^{(u2)}-1)}<\Gamma_{H_{i_c0}^{(u1)}}/(\Gamma_{(H_{(2c-1)0}^{(u3)}-1)}+1)\}$. The cardinal of $\mathcal{H}_{i_c(2c-1)0}$ is $\sum_{z=1}^{K^2}k_z$, where $k_z\le\lceil z/K\rceil$ is the number of states that $H_{i_c0}^{(u2)}$ can take when $H_{i_c0}^{(u1)}=\lceil z/K\rceil$ and $H_{(2c-1)0}^{(u3)}=z-\lfloor z/K\rfloor K$. The value of k_z depends on the values of the AMC threshold Γ_k, $k\in\{1,\ldots,K\}$.

Proof: The proof of (1) is straightforward from definition. The proof of (2) follows from the fact that $H_{ij}^{(u1)}$ and $H_{ij}^{(u2)}$ depend on the values of γ_{ij} and $SINR_{ij}^{(u2)}$ of link (i,j), respectively. Obviously, $SINR_{ij}^{(u2)}\le\gamma_{ij}$. Similarly, the proof of (3) follows from the fact that $H_{i_c0}^{(u1)}$ and $H_{i_c0}^{(u2)}$ depend on the values of γ_{i_c0} and $SINR_{i_c0}^{(u2)}$ of link $(i_c,0)$, respectively. Moreover, $H_{(2c-1)0}^{(u3)}$ depends on the value of $\gamma_{(2c-1)0}$ of link $(2c-1,0)$. Therefore, we have $\gamma_{i_c0}\in[\Gamma_{(H_{i_c0}^{(u1)}-1)},\Gamma_{H_{i_c0}^{(u1)}})$, $\gamma_{(2c-1)0}\in[\Gamma_{(H_{(2c-1)0}^{(u3)}-1)},\Gamma_{H_{(2c-1)0}^{(u3)}})$, and $SINR_{i_c0}^{(u2)}=(\gamma_{i_c0}/(1+\gamma_{(2c-1)0}))\in[\Gamma_{(H_{i_c0}^{(u2)}-1)},\Gamma_{H_{i_c0}^{(u2)}})$. From the above inequalities, we can derive the restrictions on the values of the individual CSIs in the joint space. Specifically, while both $H_{i_c0}^{(u1)}$ and $H_{(2c-1)0}^{(u3)}$ ranges from 1 to K, the values of $H_{i_c0}^{(u2)}$ has to meet the inequalities in 3). ■

2) QSI Transition Probability: According to (3), the conditional probability of $Q_{i,t+1}^{(c)}$ given the system state $\mathbf{S}_t$ and an action $\mathbf{a}$ can be derived as

$$\Pr\left\{Q_{i,t+1}^{(c)}|\mathbf{S}_t,\mathbf{a}\right\}=\begin{cases}\Pr\left(A_{i,t}^{(c)}=Q_{i,t+1}^{(c)}-Q_{i,t}^{(c)}+r_{i,t}^{(c)}\right) & \text{if } Q_{i,t}^{(c)}>r_{i,t}^{(c)},\ Q_{i,t+1}^{(c)}\ne N_{\mathrm{Q}}\\ \Pr\left(A_{i,t}^{(c)}=Q_{i,t+1}^{(c)}\right) & \text{if } Q_{i,t}^{(c)}\le r_{i,t}^{(c)},\ Q_{i,t+1}^{(c)}\ne N_{\mathrm{Q}}\\ \Pr\left(A_{i,t}^{(c)}\ge N_{\mathrm{Q}}-Q_{i,t}^{(c)}+r_{i,t}^{(c)}\right) & \text{if } Q_{i,t}^{(c)}>r_{i,t}^{(c)},\ Q_{i,t+1}^{(c)}=N_{\mathrm{Q}}\\ \Pr\left(A_{i,t}^{(c)}\ge N_{\mathrm{Q}}\right) & \text{if } Q_{i,t}^{(c)}\le r_{i,t}^{(c)},\ Q_{i,t+1}^{(c)}=N_{\mathrm{Q}}.\end{cases}\tag{9}$$

According to (1) and (2), the value of $r_{i,t}^{(c)}$ in (8) is dependent on the link set constraint $\mathcal{L}_c$, the corresponding uplink or downlink scheduling action $\mathbf{a}_*$ for queue $q_i^{(c)}$, and the data rate $r_{ij,t}^{(u)}$ of link $(i,j)\in\mathcal{L}_c$ assuming RRG $\mathcal{B}_u, u\in\mathcal{U}_{ij}$ is scheduled. $r_{ij,t}^{(u)}$ is determined in turn by the channel state $H_{ij,t}^{(u)}$.

The value of $\Pr.(A_{i,t}^{(c)}=arr)$ in (8) depends on the queue $q_i^{(c)}\in\Theta$. As discussed in the "Network Model" section, if node i is the source node of connection c, its data arrival process equals $A_{c,t}$, which has a general distribution $\Pr.(A_c)$ with mean $\lambda_c\Delta T$. Otherwise, for any $q_0^{(c)}$ where $c\in\mathcal{C}_{\mathrm{D2}}\bigcup\mathcal{C}_{\mathrm{D3}}$, its data arrival process depends on the data departure process of link $(2c-1,0)$ in the uplink transmission. Therefore, we examine the probability that arr units of data are transmitted via link $(2c-1,0)$ when the system state is $\mathbf{S}$. For any RRG $u\in\mathcal{U}_{(2c-1)0}$, the selection probability $\phi_{\mathbf{S}}(\mathbf{a}_{\mathrm{u}}^{(u)})$ of RRG $\mathcal{B}_u$ can be derived from (6). When RRG $\mathcal{B}_u$ and thus link

$$p_{\mathbf{H}_{\mathrm{u},t}}^{\mathbf{H}_{\mathrm{u},t+1}}=\begin{cases}p_{H_{12,t}^{(1)},H_{12,t}^{(3)}}^{H_{12,(t+1)}^{(1)},H_{12,(t+1)}^{(3)}}\,p_{H_{30,t}^{(2)},H_{30,t}^{(3)}}^{H_{30,(t+1)}^{(2)},H_{30,(t+1)}^{(3)}} & \text{D2D Mode}\\ p_{H_{10,t}^{(4)}}^{H_{10,(t+1)}^{(4)}}\,p_{H_{20,t}^{(2)}}^{H_{20,(t+1)}^{(2)}} & \text{Cellular Mode}\\ p_{H_{12,t}^{(1)},H_{12,t}^{(3)}}^{H_{12,t+1}^{(1)},H_{12,t+1}^{(3)}}\,p_{H_{30,t}^{(2)},H_{30,t}^{(3)},H_{10,t}^{(4)}}^{H_{30,(t+1)}^{(2)},H_{30,(t+1)}^{(3)},H_{10,(t+1)}^{(4)}} & \text{Hybrid Mode}\end{cases}\tag{8}$$

$(2c-1,0)$ is scheduled in system state $\mathbf{S}$, the units of data transmitted over link $(2c-1,0)$ during a time slot is

$$T_{(2c-1)0}=\begin{cases} R_{H^{(u)}_{(2c-1)0}} & \text{if } Q^{(c)}_{2c-1}\geq R_{H^{(u)}_{(2c-1)0}} \\ Q^{(c)}_{2c-1} & \text{if } Q^{(c)}_{2c-1}< R_{H^{(u)}_{(2c-1)0}}. \end{cases} \tag{10}$$

Otherwise, the units of data transmitted over link $(2c-1,0)$ during a time slot is 0 when it is not scheduled. Therefore, we have (11), shown at the bottom of the page. The QSI transition probability $\Pr.\{\mathbf{Q}_{t+1}|\mathbf{S}_t,\mathbf{a}\}$ can be derived as the product of $\Pr.\{Q^{(c)}_{i,t+1}|\mathbf{S}_t,\mathbf{a}\}$ over all queues $q^{(c)}_i\in\Theta$.

Finally, given a randomized control policy Ω, we can derive the system state transition probability as

$$\Pr.\{\mathbf{S}_{t+1}|\mathbf{S}_t,\Omega(\mathbf{S}_t)\}=\sum_{a\in\mathcal{A}}\Pr.\{\mathbf{S}_{t+1}|\mathbf{S}_t,\mathbf{a}\}\phi_{\mathbf{S}_t}(\mathbf{a}_{\mathrm{u}})\phi_{\mathbf{S}_t}(\mathbf{a}_{\mathrm{d}}) \tag{12}$$

Let $\mathbf{S}^{(y)}$ denote the y-th system state within the state space. Define the transition probability matrix $\mathbf{P}^{\Omega}=[\Pr.\{\mathbf{S}_{t+1}=\mathbf{S}^{(y)}|\mathbf{S}_t=\mathbf{S}^{(z)},\Omega(\mathbf{S}^{(z)})\}],y,z\in\{1,\ldots,|\mathcal{S}|\}$ and the steady-state probability matrix $\boldsymbol{\pi}^{\Omega}=[\pi^{\Omega}_{\mathbf{S}^{(z)}}],z\in\{1,\ldots,|\mathcal{S}|\}$, where $\pi^{\Omega}_{\mathbf{S}^{(z)}}=\lim_{t\to\infty}\Pr.\{\mathbf{S}_t=\mathbf{S}^{(z)}\}$. Each element of the transition probability matrix $\mathbf{P}^{\Omega}$ can be derived from (12). Then, the stationary distribution of the ergodic process $\{\mathbf{S}_t\}_{t=0,1,\ldots}$ can be uniquely determined from the balance equation.

B. Approximate Solution of Steady-State Probabilities: Model Decomposition and Iteration Approach

The computation of the steady-state distribution of $\mathbf{S}_t$ above faces the challenge of exponentially enlarged state space, which makes it unacceptable for a large number of connections. Specifically, the cardinality of the system state space is $|\mathcal{S}|=|\mathcal{H}|(N_{\mathrm{Q}}+1)^{|\Theta|}$, where $|\mathcal{H}|$ grows exponentially with the number of links. Since the number of links and queues $L=|\Theta|+|\mathcal{C}_{\mathrm{D3}}|=C+|\mathcal{C}_{\mathrm{D2}}|+2|\mathcal{C}_{\mathrm{D3}}|$, the system state space grows exponentially with the number of connections C. In order to solve the above problem, model decomposition and iteration approach is introduced to simplify the analysis.

1) Model Decomposition: We decompose the QM for the general network model into $|\Theta|$ submodels (SQMs), where each SQM (i,c) represents the queuing behavior of a single queue $q^{(c)}_i$. Define $\mathbf{S}^{(c)}_{i,t}:=(\mathbf{H}^{(c)}_{i,t},Q^{(c)}_{i,t})$ as the DTMC underlying SQM (i,c), where $\mathbf{H}^{(c)}_{i,t}:=\{\mathbf{H}_{ij,t}|(i,j)\in\mathcal{L}_c\}$ is a vector including the CSI of all links serving $q^{(c)}_i$. Let $\mathcal{S}^{(c)}_i$ denote the state space of SQM (i,c). By decomposition, the cardinality of the state space of submodel (i,c) reduces to $|\mathcal{S}^{(c)}_i|=(\prod_{(i,j)\in\mathcal{L}_c}\mathcal{H}_{ij})(N_Q+1)$, where the cardinality of $\mathcal{H}_{ij}$ is given in Theorem 1.

Let $\mathbf{S}^{(y)}_{(i,c)}$ denote the y-th system state within the local state space. Define the transition probability matrix of SQM (i,c) under control policy Ω by $\mathbf{P}^{\Omega}_{(i,c)}=[\Pr.\{\mathbf{S}^{(c)}_{i,t+1}=\mathbf{S}^{(y)}_{(i,c)}|\mathbf{S}^{(c)}_{i,t}=\mathbf{S}^{(z)}_{(i,c)},\Omega(\mathbf{S}^{(z)}_{(i,c)})\}],y,z\in\{1,\ldots,|\mathcal{S}^{(c)}_i|\}$. Define the steady-state probability matrix as $\boldsymbol{\pi}^{\Omega}_{(i,c)}=[\pi^{\Omega}_{\mathbf{S}^{(z)}_{(i,c)}}],z\in\{1,\ldots,|\mathcal{S}^{(c)}_i|\}$, where $\pi^{\Omega}_{\mathbf{S}^{(z)}_{(i,c)}}=\lim_{t\to\infty}\Pr.\{\mathbf{S}^{(c)}_{i,t}=\mathbf{S}^{(z)}_{(i,c)}\}$. Obviously, if each SQM can be analyzed separately by the balance equation, the steady-state distributions of the local system states of every SQM $\{\boldsymbol{\pi}^{\Omega}_{(i,c)}|q^{(c)}_i\in\Theta\}$ instead of the joint steady-state distributions of the global system states of the original QM $\boldsymbol{\pi}^{\Omega}$ can be derived. Therefore, model decomposition can significantly reduce the size of the state space in the analysis and achieve better performance in computational complexity.

However, the above decomposition is not "clean", i.e., there exist interactions between SQMs. The main reason is that the RRG scheduling action under a policy depends on the global system state instead of only the local system state of a SQM. Therefore, we cannot derive $\{\phi_{\mathbf{S}}(\mathbf{a}_*)|\mathbf{a}_*\in\mathcal{A}_*\}$ solely based on the local system state $\mathbf{S}^{(c)}_i$. However, in order to derive the transition probability matrix $\mathbf{P}^{\Omega}_{(i,c)}$, we need to determine $\phi_{\mathbf{S}}(\mathbf{a}_*)$. Therefore, the system states of the other SQMs have to be available in order to derive the steady-state distribution of a single SQM, which is impossible due to model decomposition. In order to deal with this problem, we derive the approximate selection probability of every action in the next step.

2) Transition Probability Approximation: We assume that when solving SQM (i,c), the steady-state probability matrices $\widetilde{\boldsymbol{\pi}}^{\Omega}_{(i',c')}$ of the other SQMs (i',c'), $\forall\, q^{(c')}_{i'}\in\Theta\setminus\{q^{(c)}_i\}$, have already been derived. The approximate selection probability of an action $\widetilde{\phi}_{\mathbf{S}^{(c)}_i}(\mathbf{a}_*)$ under the local system state $\mathbf{S}^{(c)}_i$ of SQM (i,c) can be derived as the expected value of the exact action selection probability $\phi_{\mathbf{S}}(\mathbf{a}_*)$ over the state space of the other SQMs. Let $\mathbf{E}^{\pi(\Omega)}[x]$ denote the expectation operation taken w.r.t. the unique steady-state distribution induced by the given policy Ω, where x is a function of the system state $\mathbf{S}$. We have

$$\Omega_*\left(\mathbf{S}^{(c)}_i\right)=\left\{\widetilde{\phi}_{\mathbf{S}^{(c)}_i}(\mathbf{a}_*)|\mathbf{a}_*\in\mathcal{A}_*\right\},\ \forall\,\mathbf{S}^{(c)}_i\in\mathcal{S}^{(c)}_i, \tag{13}$$

$$\Pr.\left(A^{(c)}_{0,t}=arr|\mathbf{S}_t\right)=\begin{cases} \phi_{\mathbf{S}_t}\left(\mathbf{a}^{(u)}_{\mathrm{u}}\right) & \text{if } \forall u\in\mathcal{U}_{(2c-1)0}, \\ & arr=R_{H^{(u)}_{(2c-1)0}} \text{ and } Q^{(c)}_{2c-1}\geq R_{H^{(u)}_{(2c-1)0}}, \\ & \text{or} \\ & arr=Q^{(c)}_{2c-1} \text{ and } Q^{(c)}_{2c-1}< R_{H^{(u)}_{(2c-1)0}}, \\ 1-\sum_{u\in\mathcal{U}_{(2c-1)0}}\phi_{\mathbf{S}_t}\left(\mathbf{a}^{(u)}_{\mathrm{u}}\right) & \text{if } arr=0 \\ 0 & \text{otherwise.} \end{cases} \tag{11}$$

where

$$\widetilde{\phi}_{\mathbf{S}_i^{(c)}}(\mathbf{a}_*) = \mathbf{E}^{\pi(\Omega)}\left[\phi_{\mathbf{S}}(\mathbf{a}_*)|\mathbf{S}_i^{(c)}\right]. \tag{14}$$

Moreover, for any D2D connection $c \in \mathcal{C}_{\mathrm{D2}} \bigcup \mathcal{C}_{\mathrm{D3}}$ in cellular RM or Hybrid RM, the local state transition probability $\Pr.\{\mathbf{S}_{0,t+1}^{(c)}|\mathbf{S}_{0,t}^{(c)}, \mathbf{a}_{\mathrm{d}}\}$ cannot be determined given a RRG scheduling action $\mathbf{a}_{\mathrm{d}}$. This is because the QSI transition probability $\Pr.\{Q_{0,t+1}^{(c)}|\mathbf{S}_{0,t}^{(c)}, \mathbf{a}_{\mathrm{d}}\}$ is dependent on the departure process of link $(2c-1, 0)$, which in turn depends on the global system state $\mathbf{S}_t$. Given the steady-state probabilities of SQM $(2c-1, c)$ $(\pi_{\mathbf{S}_{(2c-1),c}^{(z)}})$ and the approximate selection probability of RRG $\mathcal{B}_u$, $u \in \mathcal{U}_{(2c-1)0}$ under policy Ω_{u} when the local state of SQM $(2c-1, c)$ is known $(\widetilde{\phi}_{(\mathbf{S}_{(2c-1),c}^{(z)})}(\mathbf{a}_{\mathrm{u}}^{(u)}))$, we can derive the approximate arrival rate of $q_0^{(c)}$ for any D2D connection $c \in \mathcal{C}_{\mathrm{D2}} \bigcup \mathcal{C}_{\mathrm{D3}}$ in cellular RM or Hybrid RM as

$$\begin{aligned}
&\Pr.\left(A_{0,t}^{(c)} = arr\right) \\
&\approx \begin{cases}
\widetilde{\phi}_{\left(\mathbf{S}_{(2c-1),c}^{(z)}\right)}\left(\mathbf{a}_{\mathrm{u}}^{(u)}\right)\pi_{\mathbf{S}_{(2c-1),c}^{(z)}} \\
\text{if } \forall\, z \in \left\{1, \ldots, \left|\mathcal{S}_{2c-1}^{(c)}\right|\right\}, u \in \mathcal{U}_{(2c-1)0}, \\
\quad arr = R_{H_{(2c-1)0}}^{(u)} \text{ and } Q_{2c-1}^{(c)} \geq R_{H_{(2c-1)0}}^{(u)}, \text{ or} \\
\quad arr = Q_{2c-1}^{(c)} \text{ and } Q_{2c-1}^{(c)} < R_{H_{(2c-1)0}}^{(u)} \\
1 - \sum_{z=1}^{\left|\mathcal{S}_{2c-1}^{(c)}\right|} \sum_{u \in \mathcal{U}_{(2c-1)0}} \widetilde{\phi}_{\left(\mathbf{S}_{(2c-1),c}^{(z)}\right)}\left(\mathbf{a}_{\mathrm{u}}^{(u)}\right)\pi_{\mathbf{S}_{(2c-1),c}^{(z)}} \\
\text{if } arr = 0 \\
0 \\
\text{otherwise.}
\end{cases}
\end{aligned} \tag{15}$$

Therefore, we can derive the approximate state transition probability matrix $\widetilde{\mathbf{P}}_{(i,c)}^{\Omega}$ with each element as

$$\begin{aligned}
&\sum_{\mathbf{a}_* \in \mathcal{A}_*} \Pr.\left\{\mathbf{S}_{i,(t+1)}^{(c)}|\mathbf{S}_{i,t}^{(c)}, \mathbf{a}_*\right\} \widetilde{\phi}_{\mathbf{S}_{i,t}^{(c)}}(\mathbf{a}_*) \\
&= \Pr.\left\{\mathbf{H}_{i,(t+1)}^{(c)}|\mathbf{H}_{i,t}^{(c)}\right\} \sum_{\mathbf{a}_* \in \mathcal{A}_*} \Pr.\left\{Q_{i,(t+1)}^{(c)}|\mathbf{S}_{i,t}^{(c)}, \mathbf{a}_*\right\} \widetilde{\phi}_{\mathbf{S}_{i,t}^{(c)}}(\mathbf{a}_*)
\end{aligned} \tag{16}$$

and thus the approximate steady-state probability matrix $\widetilde{\boldsymbol{\pi}}_{(i,c)}^{\Omega}$ of SQM (i, c) can be computed by the balance equation.

However, if we solve the SQMs sequentially by index, the above requirement cannot be satisfied since only the steady-state solutions of SQMs $(i', c') \prec (i, c)$ are known when solving the SQM(i, c). In the following section, fixed point iteration is introduced to solve this problem.

3) Fixed Point Iteration: Let $\{\boldsymbol{\pi}_{(i,c)}^{\Omega}|q_i^{(c)} \in \Theta\}$ be the vector of iteration variables of the fixed point equation

$$\left\{\boldsymbol{\pi}_{(i,c)}^{\Omega}|q_i^{(c)} \in \Theta\right\} = f\left(\left\{\boldsymbol{\pi}_{(i,c)}^{\Omega}|q_i^{(c)} \in \Theta\right\}\right). \tag{17}$$

where function f is realized by solving $|\Theta|$ submodels successively with the submodel solution method as described above. The fixed point iteration can be derived by successive substitution. We define the initial vector as $\{\boldsymbol{\pi}_{(i,c)}^{\Omega,0}|q_i^{(c)} \in \Theta\}$. Each element of $\boldsymbol{\pi}_{(i,c)}^{\Omega,0}$ can be set to an arbitrary value between 0 and 1. In the ϵ-th iteration, we have

$$\left\{\boldsymbol{\pi}_{(i,c)}^{\Omega,\epsilon}|q_i^{(c)} \in \Theta\right\} = f\left(\left\{\boldsymbol{\pi}_{(i,c)}^{\Omega,\epsilon-1}|q_i^{(c)} \in \Theta\right\}\right). \tag{18}$$

where the iteration variables are determined by the function f based on the values of the last iteration. The iteration is terminated when the differences between the iteration variables of two successive iterations are less than a certain threshold value. The convergence of the fixed point iteration can be proved according to Theorem 2 in [18], which is omitted in this paper due to space limitation.

The reduction of the computational complexity when applying the decomposition and iteration approach is substantial. Let η and n represent the number of non-zero entries of the transition probability matrix of DTMC $\mathbf{S}$ underlying the exact model and iterations for the numerical solution (e.g., Successive Over-Relaxation (SOR) method) of the exact model. Note that η is of the order $|\mathcal{S}|^2$, i.e., square of the state space of the exact model, while n depends on the spectral radius of transition probability matrix of DTMC $\{\mathbf{S}_t\}_{t=0,1,\ldots}$. Therefore, the total number of floating point operations is equal to ηn to solve the exact model [17]. For the decomposition and iteration approach, if Υ iterations are needed at the decomposition level, since $|\Theta|$ SQMs need to be analyzed at each iteration, if at the ϵ-th iteration $(1 \leq \epsilon \leq \Upsilon)$, SQM (i, c) has an underlying DTMC $\{\mathbf{S}_{i,t}^{(c)}\}_{t=0,1,\ldots}$ where there are $\eta_{(i,c)}^{(\epsilon)}$ non-zero entries in its transition probability matrix, requiring $n_{(i,c)}^{(\epsilon)}$ iterations of the numerical method for its solution, the total cost is $\sum_{q_i^{(c)} \in \Theta} \sum_{\epsilon=1}^{\Upsilon} \eta_{(i,c)}^{(\epsilon)} n_{(i,c)}^{(\epsilon)}$. Since $|\mathcal{S}|$ and η grow exponentially with the number of queues $|\Theta|$ in the exact model, their large sizes indicate how the number of integer operations and the memory requirements are extremely large as well. On the other hand, since $|\mathcal{S}_i^{(c)}|$ and $\eta_{(i,c)}^{(\epsilon)}$ remain the same irrespective of the number of queues $|\Theta|$, the execution time and memory requirements of the decomposition and iteration approach only grow linearly with $|\Theta|$.

C. Performance Metrics

Given $\boldsymbol{\pi}^{\Omega}$, the end-to-end performance measures such as the mean throughput, the average delay and the dropping probability for all the connections can be derived.

1) Average Queue Length: The average queue length of queue $q_i^{(c)}$ equals

$$\overline{Q}_i^{(c)} = \mathbf{E}^{\pi(\Omega)}\left[Q_i^{(c)}\right], \tag{19}$$

2) Mean Throughput: Denote $\overline{T}_c$ as the end-to-end mean throughput of connection $c \in \mathcal{C}$ and $\overline{T}_{ij}$ as the mean throughput of link (i, j). As every cellular uplink or downlink connection $c \in \mathcal{C}_{\mathrm{Cu}} \bigcup \mathcal{C}_{\mathrm{Cd}}$ only consists of one link, we have $\overline{T}_c = \overline{T}_{(c+D)0}$ or $\overline{T}_c = \overline{T}_{0(c+D)}$. Similarly, as a D2D connection $c \in \mathcal{C}_{\mathrm{D}}$ in D2D RM also consists of one hop, we have $\overline{T}_c = \overline{T}_{(2c-1)(2c)}$. If a D2D connection $c \in \mathcal{C}_{\mathrm{D}}$ works in Cellular RM, since the data of connection c are transmitted via a two-hop route, we have $\overline{T}_c = \min[\overline{T}_{(2c-1)0}, \overline{T}_{0(2c)}] = \overline{T}_{0(2c)}$. If a

D2D connection $c \in \mathcal{C}_{\rm D}$ works in Hybrid RM, since the data of connection c can be transmitted either via the single-hop route or the two-hop route, we have $\overline{T}_c = \overline{T}_{(2c-1)(2c)} + \overline{T}_{0(2c)}$.

According to the discussion above, we need to derive the mean throughput of related links in order to obtain the end-to-end mean throughput of a connection c. The mean throughput of a link $(i,j) \in \widetilde{\mathcal{L}}$ can be derived as

$$\overline{T}_{ij} = \mathbf{E}^{\pi(\Omega)}\left[\sum_{\mathbf{a}_* \in \mathcal{A}_*} T_{ij}\left(\mathbf{S}_i^{(c)}, \mathbf{a}_*\right)\phi_{\mathbf{S}}(\mathbf{a}_*)\right], \quad (20)$$

where

$$T_{ij}\left(\mathbf{S}_i^{(c)}, \mathbf{a}_*\right) = \begin{cases} r_{ij}\left(\mathbf{S}_i^{(c)}, \mathbf{a}_*\right) & \text{if } Q_i^{(c)} \geq r_{ij}(\mathbf{H}_{ij}, \mathbf{a}_*) \\ Q_i^{(c)} & \text{if } Q_i^{(c)} < r_{ij}(\mathbf{H}_{ij}, \mathbf{a}_*) \end{cases} \quad (21)$$

is the service rate of link (i,j), which depends on the minimum value of the channel transmission capability r_{ij} of link (i,j) and the amount of data in the queue $q_i^{(c)}$. Note that r_{ij} depends on the corresponding uplink or downlink scheduling action $\mathbf{a}_*$ and the local channel state $\mathbf{H}_{ij}$ of link (i,j).

3) Average Delay: Denote $\overline{D}_c$ as the end-to-end average delay of connection $c \in \mathcal{C}$ and $\overline{D}_i^{(c)}$ as the average delay of queue $q_i^{(c)}$. Similar to derivation of mean throughput, it is straightforward to see that $\overline{D}_c = \overline{D}_{c+D}^{(c)}$ for any cellular uplink connection $c \in \mathcal{C}_{\rm Cu}$ and $\overline{D}_c = \overline{D}_0^{(c)}$ for any cellular downlink connection $c \in \mathcal{C}_{\rm Cd}$. For any D2D connection $c \in \mathcal{C}_{\rm D}$ in D2D RM, we have $\overline{D}_c = \overline{D}_{2c-1}^{c}$. For any D2D connection $c \in \mathcal{C}_{\rm D}$ in Cellular RM, since the data are transmitted via a two-hop route, we have $\overline{D}_c = \overline{D}_{2c-1}^{(c)} + \overline{D}_0^{(c)}$. For any D2D connection $c \in \mathcal{C}_{\rm D}$ in Hybrid RM, since the data can be transmitted either via the single-hop route or the two-hop route, we have $\overline{D}_c = \overline{D}_{2c-1}^{(c)} + \overline{D}_0^{(c)}(\overline{T}_{0(2c)}/(\overline{T}_{(2c-1)(2c)} + \overline{T}_{0(2c)}))$. This is because among all the served data for connection c, $\overline{T}_{(2c-1)(2c)}/(\overline{T}_{(2c-1)(2c)} + \overline{T}_{0(2c)})$ fraction of data are transmitted via the single hop route which has an average delay of $\overline{D}_{2c-1}^{(c)}$, while $\overline{T}_{0(2c)}/(\overline{T}_{(2c-1)(2c)} + \overline{T}_{0(2c)})$ fraction of data are transmitted via the two-hop route which has an average delay of $\overline{D}_{2c-1}^{(c)} + \overline{D}_0^{(c)}$.

The average delay $\overline{D}_i^{(c)}$ for any queue $q_i^{(c)}$ can be calculated according to Little's Law as

$$\overline{D}_i^{(c)} = \overline{Q}_i^{(c)} \Big/ \sum_{(i,j)\in\mathcal{L}_c} \overline{T}_{ij}, \quad (22)$$

which is the average amount of time between the arrival and departure of a packet in queue $q_i^{(c)}$. Note that $\sum_{(i,j)\in\mathcal{L}_c} \overline{T}_{ij}$ is mean throughput of queue $q_i^{(c)}$, which is the sum of the mean throughput of all the links (i,j) serving $q_i^{(c)}$. Due to the packet dropping mechanism, $\sum_{(i,j)\in\mathcal{L}_c} \overline{T}_{ij}$ equals the effective arrival rate of queue $q_i^{(c)}$, which is the average rate at which the packets enter queue $q_i^{(c)}$.

4) Dropping Probability: Denote d_c as the dropping probability of connection $c \in \mathcal{C}$ and $d_i^{(c)}$ as the dropping probability of queue $q_i^{(c)}$. It is straightforward to see that $d_c = d_{(c+D)}^{(c)}$ for any cellular uplink connection $c \in \mathcal{C}_{\rm Cu}$ and $d_c = d_0^{(c)}$ for any cellular downlink connection $c \in \mathcal{C}_{\rm Cd}$. For any D2D connection $c \in \mathcal{C}_{\rm D}$ in D2D RM, we have $d_c = d_{(2c-1)}^{(c)}$. For any D2D connection $c \in \mathcal{C}_{\rm D}$ in Cellular RM, since the data are transmitted via a two-hop route, we have $d_c = 1 - (1 - d_{(2c-1)}^{(c)})(1 - d_0^{(c)})$. For any D2D connection $c \in \mathcal{C}_{\rm D}$ in Hybrid RM, since the data of connection c can be transmitted either via the single-hop route or the two-hop route, we have $d_c = 1 - [(1 - d_{(2c-1)}^{(c)})(1 - d_0^{(c)}(\overline{T}_{(2c-1)0}/(\overline{T}_{(2c-1)(2c)} + \overline{T}_{(2c-1)0})))]$. This is because among the packets that are successfully transmitted from queue $q_{(2c-1)}^{(c)}$, $\overline{T}_{(2c-1)(2c)}/(\overline{T}_{(2c-1)(2c)} + \overline{T}_{(2c-1)0})$ fraction of data are transmitted via the single-hop route to the destination. On the other hand, $\overline{T}_{(2c-1)0}/(\overline{T}_{(2c-1)(2c)} + \overline{T}_{(2c-1)0})$ fraction of data are transmitted via the two-hop route to queue $q_0^{(c)}$, which may be dropped with probability $d_0^{(c)}$ at queue $q_0^{(c)}$.

Let $B_{i,t}^{(c)}$ be the random variable which represents the number of dropped data of queue $q_i^{(c)}$ at time slot t with system state $\mathbf{S}_t$. Since $N_{\rm Q} + b = A_{i,t}^{(c)} + \max[0, Q_{i,t}^{(c)} - r_{i,t}^{(c)}]$, where b is the number of packets dropped during the t-th slot, we obtain (23), shown at the bottom of the page.

Then, the dropping probability $d_i^{(c)}$ of queue $q_i^{(c)}$ can be estimated as

$$\begin{aligned} d_i^{(c)} &= \frac{\text{Average \# of packets dropped in a time slot}}{\text{Average \# of packets arrived in a time slot}} \\ &= \frac{\mathbf{E}^{\pi(\Omega)}\left[\sum_{b=0}^{\infty} b \Pr.\left(B_{i,t}^{(c)} = b\right)\right]}{\bar{A}_{i,t}^{(c)}}, \end{aligned} \quad (24)$$

where $\bar{A}_{i,t}^{(c)} = \lambda_c$ if node i is the source node of connection c. On the other hand, for the D2D connection c in Cellular RM or Hybrid RM, the mean amount of data arrived to the queue on the BS for this connection equals the mean throughput of the corresponding cellular uplink, i.e., $\bar{A}_{0,t}^{(c)} = \overline{T}_{(2c-1)0,t} = \mathbf{E}^{\pi(\Omega)}[T_{(2c-1)0,t}]$.

When model decomposition and iteration approach is used, and the steady-state distributions of the local system states of every SQM $\{\boldsymbol{\pi}_{(i,c)}^{\Omega} | q_i^{(c)} \in \Theta\}$ instead of the joint steady-state distributions of the global system states of the original QM $\boldsymbol{\pi}^{\Omega}$ are derived, the above (19)–(24) are still valid, except that $\mathbf{E}^{\pi(\Omega)}[x]$ should be replaced by $\mathbf{E}^{\pi_{(i,c)}(\Omega)}[x]$, $\mathbf{S}$ replaced by $\mathbf{S}_i^{(c)}$, and $\phi_{\mathbf{S}}(\mathbf{a}_*)$ replaced by $\widetilde{\phi}_{\mathbf{S}_i^{(c)}}(\mathbf{a}_*)$.

$$\Pr.\left(B_{i,t}^{(c)} = b\right) = \sum_{\mathbf{a}\in\mathcal{A}} \Pr.\left(A_{i,t}^{(c)} = N_{\rm Q} + b - \max\left[0, Q_{i,t}^{(c)} - r_{i,t}^{(c)}\left(\mathbf{H}_i^{(c)}, \mathbf{a}_*\right)\right]\right)\phi_{\mathbf{S}}(\mathbf{a}_*). \quad (23)$$

V. Numerical Results and Discussions

We consider a wireless network employing adaptive M-ary quadrature amplitude modulation (M-QAM) with convolutional coding which has six channel states for all transmission links. The SINR thresholds for the channel states are given in Table II of [5]. We assume the Rayleigh fading channel and the number of packets transmitted in a time slot under different channel states, i.e., R_k with $k = 1, 2, 3, 4, 5, 6$ are set to 0, 1, 2, 3, 6, 9, respectively. The carrier frequency and the time slot duration ΔT are set to 2 GHz and 1 ms, respectively. The velocity of the terminals is set to be 3 km/h so that the Doppler frequency becomes 5.56 Hz. We let the buffer size $K = 10$ packets, where the packet length $B = 1080$ bits.

We simulate a circular cell with a BS (node 0) in the center. The cell radius is set to 500 m. The distance between the transmitter of node i and receiver of node j, i.e, the distance of link (i, j), is denoted by d_{ij}. We consider the path loss channel model $28 + 40 \log_{10} d[m]$ for any wireless channel between a pair of UEs, while the path loss channel model $15.3 + 37.6 \log_{10} d[m]$ for any wireless channel between the BS and a UE [12]. The transmission power of the BS and the UE are set to be 46 dBm and 23 dBm, respectively. We normalize the uplink noise power and downlink noise power, respectively, so that the SNR is 0 dB for any cellular uplink or downlink at the cell border.

The computational complexity in deriving the exact steady-state probabilities of the queuing model using the method given in Section IV-A is very large even for the simple example network in Fig. 1, where the state space size of the underlying DTMC is $8.4\text{e}8$ for Hybrid Mode. Therefore, we only perform numerical experiments using the model decomposition and iteration method as given in Section IV-B, where the largest SQM state space size is 1386 irrespective of the number of connections in the network. In order to validate the numerical results obtained by solving the decomposed Markov model using fixed point iteration, we develop a discrete-event simulation framework of a D2D communications system with dynamic packet arrivals. The simulation is run over 10^6 time slots and the time-average performance measures of every connection are obtained. In the numerical method, we set the initial steady-state probability of every state to be the same within vector $\boldsymbol{\pi}_{(i,c)}$ of every SQM (i, c). The number of iterations for convergence is 15.

Since we focus on the interference scenario where a cellular user can reuse resources with at most one D2D pair in this paper as discussed in the Introduction, numerical experiments on the example network in Fig. 1 with one D2D connection, one cellular uplink connection and one cellular downlink connection can provide many insights into the mode selection principle. This is because although our general network model can include multiple D2D or cellular connections, the resultant D2D links and cellular uplinks form multiple pairs of fixed resource reuse relationships, which can be seen as multiple copies of D2D connection 1 and cellular connection 2 in the uplink. For any D2D connection in our general network model, its optimal mode mainly depends on the local network topology consisting only of nodes and links related to the considered pair of D2D and cellular connections, such as the distance between the src. DUE and dest. DUE and the distance between the transmitters and receivers of the potential interference links. Compared with the network scenario in [9], [10], [12], [14], the example network in Fig. 1 additionally include a downlink cellular link, so that its impact to the optimal mode for the D2D connection can also be studied. Therefore, we first perform numerical experiments on the example network with varying topologies and arrival rates in Section V-A and B, respectively, so that some key observations with respect to the mode selection principles can be obtained. Next, we perform numerical experiments on a general network scenario with varying number of D2D connections and cellular uplink and downlink connections in Section V-C. Finally, we discuss the mode selection scheme design using our queuing model and numerical method in Section V-D.

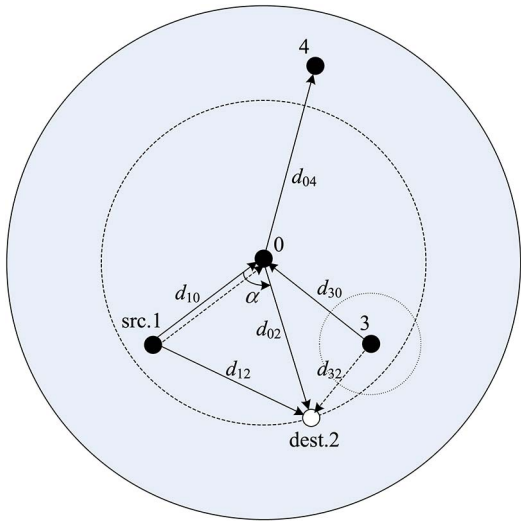

Fig. 3. The network topology for the numerical experiments.

A. Numerical Results With Varying Topologies

As illustrated in Fig. 3, we assume a pair of D2D UEs (src. node 1 and dest. nodes 2), a cellular UE with uplink transmission (node 3) and a cellular UE with downlink transmission (node 4). We perform numerical experiments with varying D2D link distance and interference conditions by fixing the positions of src. node 1, node 3, and node 4 while tuning the position of dest. node 2 so that both the distance of D2D link (1, 2) and the distance of potential interfering link (3, 2) shall change. Specifically, we set $d_{10} = d_{02} = 280$ m, $d_{30} = 200$ m, and $d_{04} = 400$ m. Moreover, the angle between links (1, 0) and (3, 0) is set to be 30°. The position of dest. node 2 can be tuned by changing the angle α between links (1, 0) and (0, 2), so that dest. node 2 rotates on the dotted circle in Fig. 3. We assume that α is positive or negative when dest. node 2 rotates anticlockwisely or clockwisely away from src. node 1. Obviously, $-180^\circ \leq \alpha \leq 180^\circ$.

We first study the performance of the semi-static RSM selection schemes, where both numerical method and simulation are performed for the D2D-NOS, D2D-OS, and Cellular Modes, and the performance of semi-statically select the NOS, OS, and CM RSMs can be obtained, respectively. We first change the

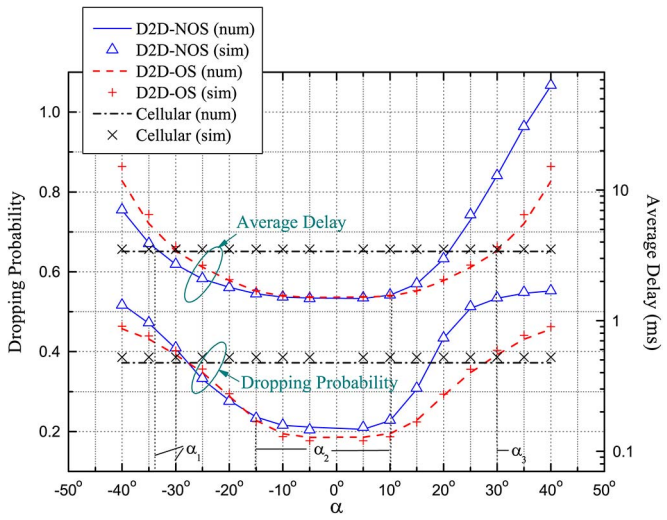

Fig. 4. Average delay and dropping probability versus the angle α between links (1, 0) and (0, 2) under MaxWeight algorithm for D2D-NOS, D2D-OS, and Cellular Modes.

TABLE III
INTERSECTING POINTS FOR THE PERFORMANCE CURVES UNDER D2D-NOS, D2D-OS AND CELLULAR MODES

Performance Measures	α_1	α_2	α_3
Average Delay	$-34°$	$10°$	$30°$
Dropping Probability	$-30°$	$-15°$	$30°$

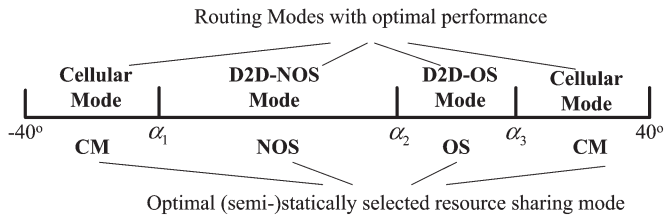

Fig. 5. The optimal routing modes partitioned by α_1, α_2, and α_3.

angle α between links (1, 0) and (0, 2) from $-40°$ to $40°$. Fig. 4 shows the numerical and simulation results for the end-to-end average packet delay and packet dropping probability averaged over the three connections under the MaxWeight scheduling algorithm, when the packet arrival rate is set to $\lambda = 5$ packets/slot. The numerical result can match the simulation trace reasonably well. For each performance metric, the curves for the three modes have three intersecting points when α equals α_1, α_2, and α_3 as summarized in Table III. When $\alpha < \alpha_1$ or $\alpha > \alpha_3$, the Cellular Mode performs better than both D2D-NOS and D2D-OS Mode. On the other hand, the D2D-NOS Mode performs the best when $\alpha_1 < \alpha < \alpha_2$ and the D2D-OS Mode performs the best when $\alpha_2 < \alpha < \alpha_3$. The regions where the D2D-NOS, D2D-OS, and Cellular Modes perform the best are illustrated in Fig. 5, which are also the regions for the optimal semi-static selection of the corresponding RSMs in terms of the corresponding performance metric.

The explanation for the above overall performance trend of both performance metrics is obvious. As expected, the performance of both D2D-NOS and D2D-OS Modes degrade with increasing $|\alpha|$ as the D2D link distance d_{12} increases, while the performance of the Cellular Mode remains unchanged as all the cellular link lengths are fixed. Although the performance of both D2D-NOS and D2D-OS Modes degrade with increasing $|\alpha|$, the performance of D2D-OS degrades symmetrically when dest. node 2 rotates anti-clockwise and clockwise with the same $|\alpha|$. On the other hand, the performance of D2D-NOS degrades faster when dest. node 2 rotates anti-clockwise as compared to clockwise. This is because the distance d_{32} of the potential interfering link I_{32} increases/decreases as dest. node 2 rotates anti-clockwise/clockwise, which causes the corresponding change in the amount of interference to D2D link (1, 2).

Although the overall performance trends are similar, the values of the intersecting points α_1 and α_2 are different for different performance metrics. Specifically, α_2 equals $10°$ and $-15°$ for average delay and dropping probability, respectively, which means that the D2D-OS mode performs better than D2D-NOS mode in terms of dropping probability but worse than D2D-NOS mode in terms of average delay when $-15° < \alpha < 10°$. This is because the D2D-OS mode uses the MaxWeight algorithm to achieve scheduling gain, while the D2D-NOS Mode does not need any scheduling algorithm as the links always transmit whenever the queues are non-empty. Moreover, the MaxWeight algorithm can achieve larger scheduling gain in terms of dropping probability than average delay. This is because the MaxWeight algorithm is designed under the infinite buffer capacity assumption with the aim to guarantee the queue lengths not drifting to infinity. When the traffic load is large and the buffer capacity is finite, the MaxWeight algorithm results in the lengths of all the queues becoming equally large. However, as the queue length is bounded by the maximum capacity K of the buffer in reality, it may be better from the average delay perspective to allocate more resources to one queue to result in its smaller delay while leaving the packet delay of the other queue be bounded by the maximum value. Also note that α_1 equals $-34°$ and $-30°$ for average delay and dropping probability, respectively, which means that the Cellular mode performs better than D2D-NOS mode in terms of dropping probability but worse than D2D-NOS mode in terms of average delay when $-34° < \alpha < -30°$. The explanation is similar with above since the Cellular mode also uses the MaxWeight algorithm. From the above observations, we can draw the conclusion that *the optimal RSM is impacted by the scheduling algorithm and the considered performance metric when semi-statically selected.*

Next, we focus on contrasting the performance of dynamic RSM selection schemes with that of the optimal semi-statically selected RSM. Fig. 6 shows the numerical and simulation results of the end-to-end average delay and dropping probability of D2D-Dynamic and Hybrid-Dynamic Modes under MaxWeight scheduling algorithm with arrival rate $\lambda = 5$ packets/slot, when the angle α between links (1, 0) and (0, 2) rotates between $-40°$ to $40°$. To provide a comparison baseline, we also illustrate the optimal performance of D2D-NOS, D2D-OS, and Cellular Modes under MaxWeight algorithm with varying α in Fig. 6, which is a synthesis of the performance curves in Fig. 4. As expected, the D2D-Dynamic Mode performs better than that of the optimal semi-static scheme when $-30° < \alpha < 30°$, which roughly corresponds to the region where D2D-NOS/D2D-OS Mode performs better

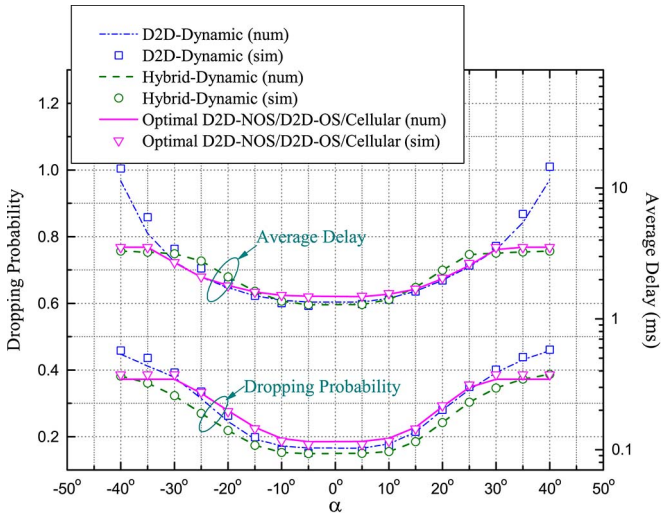

Fig. 6. Average delay and dropping probability versus the angle α between links (1, 0) and (0, 2) under MaxWeight scheduling algorithm for D2D-Dynamic, Hybrid-Dynamic, and the optimal semi-static mode selection scheme.

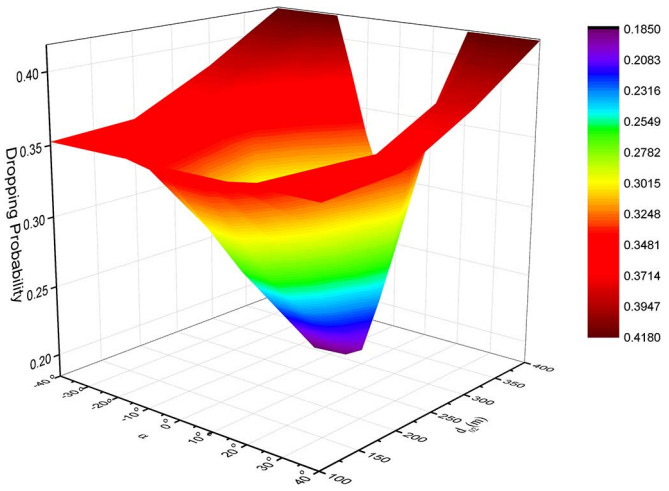

Fig. 7. Dropping probability of the optimal semi-statically selected RSM versus the angle α between links (1, 0) and (0, 2) and the distance of link (0, 2) (d_{02}) under MaxWeight scheduling algorithm.

than Cellular Mode. The largest performance gain in dropping probability achieved by D2D-Dynamic Mode (10%–15%) lies in region $-15^\circ < \alpha < 5^\circ$. From Fig. 4, we observe that the performance of D2D-NOS and D2D-OS Modes are quite close in this region, which means that D2D-Dynamic Mode can better exploit the channel variations opportunistically by dynamic selection of NOS and OS resource sharing modes. Note that from Fig. 4, the performance of D2D-NOS and D2D-OS Modes are also quite close when $-30^\circ < \alpha < -15^\circ$. However, the performance gain in dropping probability achieved by D2D-Dynamic Mode is small in this region and decreases with increasing $|\alpha|$ from Fig. 6. This is because the performance gain of D2D-Dynamic Mode depends on exploiting the dynamic channel variations of the potential interfering links, while the channel gain of potential interfering link I_{32} becomes quite small when $-30^\circ < \alpha < -15^\circ$ and decreases with increasing $|\alpha|$ due to the increasing distance between node 3 and dest. node 2. Fig. 6 further shows that the Hybrid-Dynamic Mode constantly performs better in dropping probability than both the optimal semi-static mode selection scheme and the D2D-Dynamic Mode with varying α, as it dynamically select the three RSMs in each time slot. It achieves the largest performance gain over the optimal semi-static mode selection scheme in dropping probability (20%–25%) when $-20^\circ < \alpha < -30^\circ$, which roughly corresponds to the region where the performance of Cellular, D2D-NOS and D2D-OS Modes are closest. However, when $|\alpha| = 40^\circ$, the performance gain of Hybrid-Dynamic Mode becomes negaligible and further numerical results reveal that the performance of Hybrid-Dynamic Mode and Cellular Mode are approximately the same if we increase $|\alpha|$ beyond 40°. This is because the channel gain of the D2D link (1, 2) is too small due to the large distance between src. node 1 and dest. node 2, so that the cellular link (1,0) is always selected by the Hybrid-Dynamic Mode to serve the D2D connection. From Fig. 6, we can also observe that the Hybrid-Dynamic Mode performs worse than the optimal semi-static mode selection scheme in average delay when $-30^\circ < \alpha < -5^\circ$ and $15^\circ < \alpha < 25^\circ$. From the above discussion, this is not surprising since the MaxWeight algorithm sacrifies the delay performance in order to achieve better dropping probability performance. Based on the above observations, we can draw the conclusion that *the performance gain of a dynamic RSM selection scheme over its corresponding optimal semi-statically selected RSM is also impacted by the scheduling algorithm and the considered performance metric*. Moreover, *the performance gain of a dynamic RSM selection scheme decreases as the performance gap between the corresponding RSMs increases when they are semi-statically selected, and the performance gain of D2D-Dynamic Mode is small when the interference between the D2D link and cellular link pair with resource reuse is small*.

In the above numerical experiments, we fix the distance of link (0, 2) (d_{02}) to be 280 m and rotate it in circle. Now we change the distance of link (0, 2) from 100 m to 400 m in a step of 100 m. The numerical results of the performance variation in dropping probability of the optimal semi-statically selected RSM with the changing position of dest. node 2 is shown in Fig. 7. We observe that better performance is achieved when the value of α is small irrespective of the distance of link (0, 2). This is because the channel condition of D2D link (1, 2) is good when α is small, so that the D2D-OS or D2D-NOS Mode is chosen providing performance gain over the Cellular Mode. However, when the value of α is large and the D2D link is always in poor channel condition, the Cellular Mode has to be chosen.

Fig. 8 illustrates the optimal semi-statically selected RSM with the changing position of dest. node 2 by different colors, where the X-axis is the angle α between links (1, 0) and (0, 2), while the Y-axis is the distance of link (0, 2) (d_{02}). We first focus on the selection between Cellular Mode and D2D-OS/D2D-NOS Mode. When the distance of link (0, 2) increases with a fixed value of α, the performance of the Cellular Mode will degrade. This explains why the Cellular Mode is always selected when $-40^\circ < \alpha < 40^\circ$ if $d_{02} = 100$ m, while the D2D-NOS or D2D-OS Mode is selected instead when $-20^\circ < \alpha < 25^\circ$ or

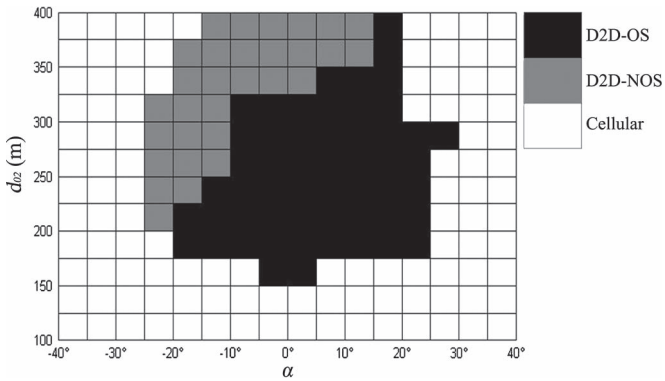

Fig. 8. The optimal semi-statically selected RSM versus the angle α between links (1, 0) and (0, 2) and the distance of link (0, 2) (d_{02}) under MaxWeight scheduling algorithm.

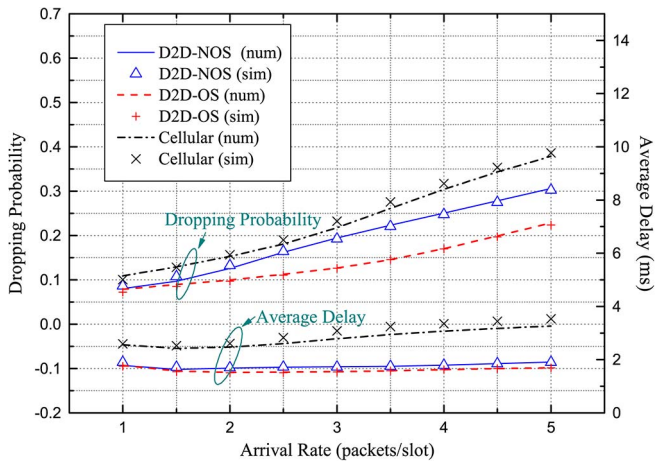

Fig. 9. Average delay and dropping probability versus arrival rate under MaxWeight scheduling algorithms $(\alpha = 15^\circ)$ for D2D-NOS, D2D-OS, and Cellular Modes.

$-25^\circ < \alpha < 30^\circ$ if $d_{02} = 200$ m or $d_{02} = 300$ m, respectively. However, when d_{02} increases to 400 m, the D2D-NOS or D2D-OS Mode is selected in a smaller α region, i.e., $-15^\circ < \alpha < 20^\circ$, compared to when d_{02} equals 200 m or 300 m, although the performance of the Cellular Mode is the worst when $d_{02} = 400$ m. This is because the distance of D2D link (1, 2) (d_{12}) also changes when the distance of link (0, 2) varies with fixed α and achieves the minimum value when $d_{02} = d_{10}\cos|\alpha|$. Since we set $d_{10} = 280$ m and $|\alpha|$ is small when D2D-NOS or D2D-OS Mode is likely to be chosen, D2D link distance d_{12} achieves the minimum value when d_{02} is a little smaller than 280 m. Therefore, when d_{02} increases to 400 m, the D2D link distance d_{12} also increases to a large value, which makes the D2D-NOS or D2D-OS Mode performs even worse than the Cellular Mode. It can be observed from Fig. 7 that the performance of the optimal semi-statically selected RSM is worse when d_{02} increases beyond 200 m, which is due to the fact that both the D2D link (1, 2) and cellular link (0, 2) have worse channel conditions. Now we turn our attention to the selection between D2D-OS and D2D-NOS Modes. Note that the distance of the potential interfering link I_{32} (d_{32}) will also change with varying d_{02} when the value of α is fixed. Similar to d_{12}, d_{32} achieves the minimum value when $d_{02} = d_{30}\cos(|30 - \alpha|)$. Since we set $d_{30} = 200$ m, the minimum value of d_{32} is achieved when $d_{02} < 200$ m. Therefore, the value of d_{32} grows larger when d_{02} increases beyond 200 m, which means that the interference from the Cellular UE (node 3) to the D2D UE (dest. node 2) becomes weaker. Therefore, it can be observed from Fig. 8 that the D2D-NOS Mode is more likely to be selected with increasing d_{02}. For example, D2D-NOS is not selected at all when α ranges from -40° to 40° if $d_{02} = 200$ m, while it is selected when $-15^\circ < \alpha < 15^\circ$ if $d_{02} = 400$ m. We only studied how the distance of link (0, 2) (d_{02}) affects performance in the above experiments. This is because the insights obtained by varying d_{02} can be used to explain how the distance variation of other links affects performance. For example, it is straightforward to see that when the angle α is fixed, varying the distance of link (1, 0) (d_{10}) also affects the D2D link distance d_{12} but has no impact on the distance of interference link I_{32} (d_{32}), which means that varying d_{10} affects selection between Cellular Mode and D2D-OS/D2D-NOS Mode in a similar way as varying d_{02}, but it will not affect the selection between D2D-OS Mode and D2D-NOS Mode. On the other hand, since the distance variation of link (3, 0) (d_{30}) will impact d_{32} but not d_{12}, the selection between D2D-OS and D2D-NOS Modes are affected by the variation of d_{30} in a similar way as varying d_{02}, but the selection between Cellular Mode and D2D-OS/D2D-NOS Mode will not be impacted.

B. Numerical Results With Varying Arrival Rates

We fix the angle $\alpha = 15^\circ$, and the variations in end-to-end average delay and dropping probability with packet arrival rate are presented in Fig. 9 for the D2D-NOS, D2D-OS, and Cellular Modes under MaxWeight scheduling algorithm. When the arrival rate λ is large, the D2D-OS Mode performs better than D2D-NOS Mode especially in terms of dropping probability, which means that the reuse gain cannot compensate for the reduction in spectral efficiency due to interference. However, when the arrival rate λ is small, we observe that the D2D-NOS and D2D-OS Modes perform similar. This is because there are larger opportunities under light traffic load that one of the two queues for the D2D link and Cellular uplink is empty, so that the other queue can transmit at full rate without interference no matter in D2D-NOS or D2D-OS Mode. We also observe an increase in the performance gap between Cellular Mode and D2D-OS/D2D-NOS Mode with increasing λ. This is because when λ is large, the performance of connection 3 is much worse in Cellular Mode compared to that in D2D-NOS/D2D-OS Mode, as some of the downlink radio resources have to be allocated to connection 1 in the Cellular Mode. However, when λ is small, this "hop gain" achieved by the D2D-NOS/D2D-OS Mode decreases as there are decreasing opportunities that both queues Q_0^1 and Q_0^3 are non-empty at the same time. From the above discussion, *the relative performance of the semi-static RSM selection schemes are affected by the arrival rate*.

We now compare the performance in terms of dropping probability of the D2D-Dynamic Mode (resp. Hybrid-Dynamic Mode) and the optimal semi-statically selected mode under

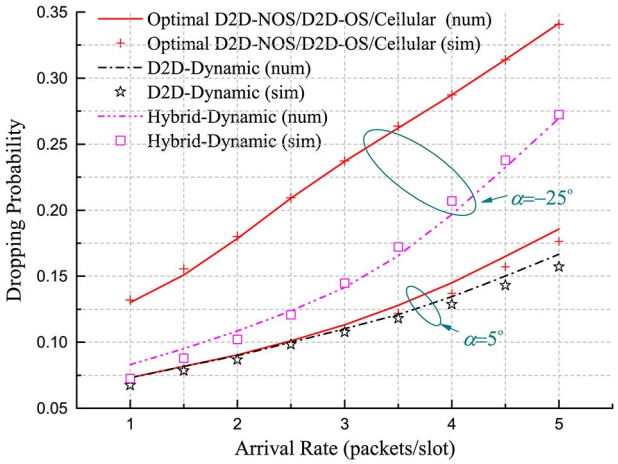

Fig. 10. Dropping probability versus arrival rate under MaxWeight scheduling algorithms for D2D-Dynamic Mode and optimal semi-statically selected RSM when $\alpha = 5^\circ$ and Hybrid-Dynamic Mode and optimal semi-statically selected RSM when $\alpha = -25^\circ$.

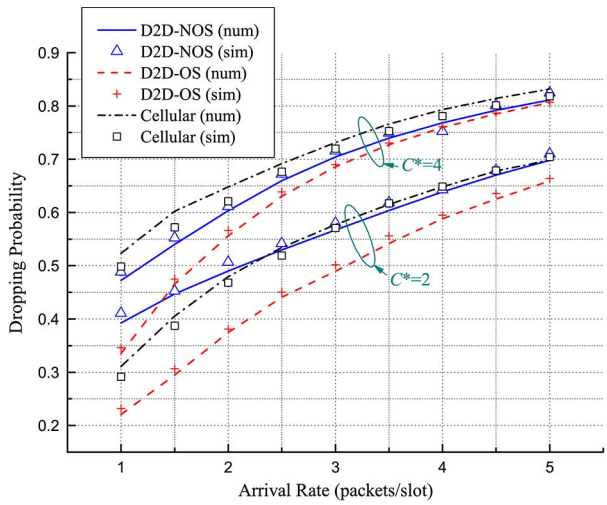

Fig. 11. Dropping probability versus arrival rate under MaxWeight scheduling algorithms ($\alpha = 15^\circ$) for D2D-NOS, D2D-OS, and Cellular Modes, when the number of D2D connection, cellular uplink connection, and cellular downlink connection are set to $\mathcal{C}_{\rm D} = \mathcal{C}_{\rm Cu} = \mathcal{C}_{\rm Cd} = C^* = 2$ or 4.

varying arrival rates with a fixed angle $\alpha = 5^\circ$ (resp. $\alpha = -25^\circ$). These two values of α are selected because it can be observed from Fig. 5 that they correspond to the angles when the respective dynamic mode selection schemes achieve the largest performance gain. Fig. 10 shows that the performance gain of D2D-Dynamic Mode increases with increasing arrival rate, since there are larger opportunities that the queues are non-empty in order to achieve the opportunistic scheduling gain. On the other hand, the performance gain of the Hybrid-Dynamic Mode is not much impacted by the varying arrival rates, since the gain mainly comes from exploiting the channel variations of three links (1, 2), (1, 0), and (3, 0) for opportunistic scheduling instead of only two links (1, 2) (or (1, 0)) and (3, 0). However, since links (1, 2) and (1, 0) serve the same queue $q_1^{(1)}$, the increasing arrival rate has the same impact on the scheduling gains of Hybrid-Dynamic Mode and the optimal semi-statically selected mode.

C. Numerical Results With Varying Link Numbers

The above numerical experiments are performed on the network topology in Fig. 3 with one D2D connection, one cellular uplink connection, and one cellular downlink connection. In this section, we illustrate the performance in terms of dropping probability of the semi-static RSM selection schemes with multiple D2D connections and cellular connections. Fig. 11 shows the numerical and simulation results when the number of D2D connections $\mathcal{C}_{\rm D}$, the number of cellular uplinks connections $\mathcal{C}_{\rm Cu}$, and the number of cellular downlink connections $\mathcal{C}_{\rm Cd}$ are all set to 2 and 4. Note that when $\mathcal{C}_{\rm D} = \mathcal{C}_{\rm Cu} = \mathcal{C}_{\rm Cd} = C^*$, there are $4C^* + 1$ nodes and $5C^*$ links in the network. It can be observed that the numerical results match reasonably well with the simulation.

D. Discussion on Mode Selection Scheme Design

Our queuing model and numerical method can be used for the design of mode selection scheme under non-saturated traffic model. As a simple example, before a pair of D2D UEs starts to setup a connection, the BS can estimate the approximate average end-to-end performance of this new connection under every communcations mode by applying our numerical method to the corresponding queuing model. When the performance in terms of the considered performance metric under one of the communications mode is better than those of the other modes, we can select this mode and set the corresponding link constraint set for scheduling algorithm. Since the dynamic RSM selection schemes involves more scheduling effort and signaling overhead than the semi-static RSM selection schemes, a threshold can be set so that the dynamic RSM selection scheme is only chosen when its performance gain over the optimal semi-static scheme is above the threshold. In this way, we achieve the desired tradeoff between computation/communications overhead and performance by tuning the threshold value. In the above example, the D2D connection and cellular connections are given the same priority. When the cellular connections are given larger priorities, we can also select the mode in which the estimated average delay or dropping probability of the D2D connection is optimized while those of the cellular connections satisfy their QoS requirements. Moreover, our QM can include scheduling algorithms that are delay optimal or with delay constraint. Our numerical method can also be used to periodically perform offline optimization to select communication modes for all the existing D2D connections.

VI. Conclusion

In this paper, we have defined three canonical routing modes for D2D communications underlaying cellular networks, which can be combined with different resource allocation restrictions to represent the semi-static and dynamic selections of the three resource sharing modes. We have developed the queuing model and proposed an exact and an approximate numerical methods to investigate the performance of D2D communications under

different routing modes with dynamic data arrival and finite-length queuing. The approximate numerical method has been validated by means of simulations. Our simulation results have demonstarted that the optimal resource sharing mode for a D2D pair is impacted by its packet arrival rate, scheduling algorithm, and the considered performance metric. Moreover, the performance gain by dynamically selecting a resource sharing mode per time slot decreases as the performance gap between the candidate resource sharing modes increases when they are semi-statically selected, and the performance gain by dynamically selecting the OS and NOS resource sharing modes decreases with decreasing interference between the D2D link and cellular link pair with resource reuse. Our performance analysis can also be used for mode selection under bursty traffic.

For broadband communications scenario with frequency-selective fading channels, since the frequency-selective fading channels can be turned into multiple parallel flat fading channels by the Orthogonal Frequency Division Multiplex (OFDM) technique, the channel state space in our FSMC model may grow with the increasing number of flat fading channels corresponding to increasing system bandwidth. Therefore, we will extend our numerical method for frequency-selective fading channels using colored Stochastic Petri Nets for state aggregation. Nevertheless, the insights derived from the numerical results based on the narrowband model should still apply in the broadband scenario. Although we assume that packet arrival process is i.i.d. over time slots following general distribution, our queuing models can be extended to Batch Markovian Arrival Process (BMAP), which is a very general arrival process that can capture correlation (i.e., burstiness) in process. The extension method is similar to that in [7] and is omitted in this paper due to space limitation. Other possible research directions include extending our queuing model to characterize the impact of inaccurate CSI feedback and to study the interference scenario between a cellular link and multiple D2D links. Our research work should provide some useful insight for the design and optimization of mode selection schemes considering dynamic packet arrival. And the analysis outlined here should be useful to industrial machine-to-machine (M2M) networks where e.g., sensors need to communicate quickly and directly with actuators.

REFERENCES

[1] L. Lei, Z. Zhong, C. Lin, and X. Shen, "Operator controlled device-to-device communications in LTE-advanced networks," *IEEE Wireless Mag.*, vol. 19, no. 3, pp. 96–104, Jun. 2012.

[2] G. Fodor *et al.*, "Design aspects of network assisted device-to-device communications," *IEEE Commun. Mag.*, vol. 50, no. 3, pp. 170–177, Mar. 2012.

[3] M. S. Corson *et al.*, "Toward proximity-aware internet working," *IEEE Wireless Commun.*, vol. 17, no. 6, pp. 26–33, Dec. 2010.

[4] K. Doppler, M. Rinne, C. Wijting, C. B. Ribeiro, and K. Hugl, "Device-to-device communication as an underlay to LTE-advanced networks," *IEEE Commun. Mag.*, vol. 47, no. 12, pp. 42–49, Dec. 2009.

[5] Q. Liu, S. Zhou, and G. B. Giannakis, "Queuing with adaptive modulation and coding over wireless links: Cross-layer analysis and design," *IEEE Trans. Wireless Commun.*, vol. 50, no. 3, pp. 1142–1153, May 2005.

[6] L. Lei, C. Lin, J. Cai, and X. Shen, "Performance analysis of opportunistic wireless schedulers using stochastic Petri nets," *IEEE Trans. Wireless Commun.*, vol. 7, no. 4, pp. 5461–5472, Apr. 2009.

[7] L. Le and E. Hossain, "Tandem queue models with applications to QoS routing in multihop wireless networks," *IEEE Trans. Mobile Comput.*, vol. 7, no. 8, pp. 1025–1040, Aug. 2008.

[8] L. Lei, Y. Zhang, X. Shen, C. Lin, and Z. Zhong, "Performance analysis of device-to-device communications with dynamic interference using stochastic Petri nets," *IEEE Trans. Wireless Commun.*, vol. 12, no. 12, pp. 6121–6141, Dec. 2013.

[9] C.-H. Yu, K. Doppler, C. B. Ribeiro, and O. Tirkkonen, "Resource sharing optimization for device-to-device communication underlaying cellular networks," *IEEE Trans. Wireless Commun.*, vol. 10, no. 8, pp. 2752–2763, Aug. 2011.

[10] K. Doppler, C.-H. Yu, C. B. Ribeiro, and P. Janis, "Mode selection for device-to-device communication underlaying an LTE-advanced network," in *Proc. IEEE WCNC*, Apr. 2010, pp. 1–6.

[11] C.-P. Chien, Y.-C. Chen, and H.-Y. Hsieh, "Exploiting spatial reuse gain through joint mode selection and resource allocation for underlay device-to-device communications," in *Proc. 15th Int. Symp. WPMC*, Sep. 2012, pp. 80–84.

[12] M. Jung, K. Hwang, and S. Choi, "Joint mode selection and power allocation scheme for power-efficient Device-to-Device (D2D) communication," in *Proc. IEEE 75th Veh. Technol. Conf. Spring*, 2012, pp. 1–5.

[13] M. Zulhasnine, C. Huang, and A. Srinivasan, "Efficient resource allocation for device-to-device communication underlaying LTE network," in *Proc. IEEE Wireless Commun. Netw. Conf.*, 2010, pp. 368–375.

[14] H. Wang and X. Chu, "Distance-constrained resource-sharing criteria for device-to-device communications underlaying cellular networks," *Electron. Lett.*, vol. 48, no. 9, pp. 528–530, Apr. 2012.

[15] M. Andrews, "A survey of scheduling theory in wireless data networks," in *Wireless Communications*, vol. 143. New York, NY, USA: Springer-Verlag, 2007, ser. The IMA Volumes in Mathematics and Its Applications, pp. 1–17.

[16] L. Georgiadis, M. J. Neely, and L. Tassiulas, "Resource allocation and cross-layer control in wireless networks," *Found. Trends Netw.*, vol. 1, no. 1, pp. 1–144, Apr. 2006.

[17] G. Ciardom and K. S. Trivedi, "A decomposition approach for stochastic reward net models," *Perform. Eval.*, vol. 18, no. 1, pp. 37–59, Jul. 1993.

[18] V. Mainkar and K. S. Trivedi, "Fixed point iteration using stochastic reward nets," in *Proc. 6th Int. Workshop Petri Nets Perform. Models*, 1995, pp. 21–30.

[19] P. A. Bello, "Characterization of randomly time-variant linear channels," *IEEE Trans. Commun. Syst.*, vol. CS-11, no. 4, pp. 360–393, Dec. 1963.

[20] P. Sadeghi, R. A. Kennedy, P. B. Rapajic, and R. Shams, "Finite-state markov modeling of fading channels—A survey of principles and applications," *IEEE Signal Process. Mag.*, vol. 25, no. 5, pp. 57–80, Sep. 2008.

Lei Lei received the B.S. and Ph.D. degrees in telecommunications engineering from Beijing University of Posts and Telecommunications, Beijing, China, in 2001 and 2006, respectively. From July 2006 to March 2008, she was a Postdoctoral Fellow with the Department of Computer Science, Tsinghua University, Beijing. From April 2008 to August 2011, she was with the Wireless Communications Department, China Mobile Research Institute. Since September 2011, she has been an Associate Professor with the State Key Laboratory of Rail Traffic Control and Safety, Beijing Jiaotong University, Beijing. Her current research interests include performance evaluation, quality of service, and radio resource management in wireless communication networks.

Xuemin (Sherman) Shen (M'97–SM'02–F'09) received the B.Sc. degree from Dalian Maritime University, Dalian, China, in 1982 and the M.Sc. and Ph.D. degrees from Rutgers University, Piscataway, NJ, USA, in 1987 and 1990, respectively. From 2004 to 2008, he was the Associate Chair for Graduate Studies with the Department of Electrical and Computer Engineering, University of Waterloo, Waterloo, ON, Canada, where he is currently a Professor and the University Research Chair. He is a coauthor/editor of six books, and has published more than 600 papers and book chapters in wireless communications and networks, control, and filtering. His research interests include resource management in interconnected wireless/wired networks, wireless network security, social networks, smart grid, and vehicular *ad hoc* and sensor networks. Dr. Shen is an elected member of the IEEE Communication Society Board of Governors and the Chair of Distinguished Lecturer Selection Committee. He served as the Technical Program Committee Chair/Co-Chair for IEEE Infocom'14 and IEEE VTC'10 Fall, as the Symposia Chair for IEEE ICC'10, as the Tutorial Chair for IEEE VTC'11 Spring and IEEE ICC'08, as the Technical Program Committee Chair for IEEE Globecom'07, as the General Cochair for Chinacom'07 and QShine'06, as the Chair for IEEE Communications Society Technical Committee on Wireless Communications, and P2P Communications and Networking. He also serves/served as the Editor-in-Chief for IEEE NETWORK, *Peer-to-Peer Networking and Application*, and *IET Communications*; as a Founding Area Editor for IEEE TRANSACTIONS ON WIRELESS COMMUNICATIONS; as an Associate Editor for IEEE TRANSACTIONS ON VEHICULAR TECHNOLOGY, *Computer Networks*, and *ACM/Wireless Networks*, etc.; and as a Guest Editor for IEEE JOURNAL ON SELECTED AREAS IN COMMUNICATIONS, IEEE WIRELESS COMMUNICATIONS, IEEE COMMUNICATIONS MAGAZINE, and*ACM Mobile Networks and Applications*, etc. Dr. Shen received the Excellent Graduate Supervision Award in 2006 and the Outstanding Performance Award in 2004, 2007, and 2010 from the University of Waterloo; the Premier's Research Excellence Award (PREA) in 2003 from the Province of Ontario, Canada; and the Distinguished Performance Award in 2002 and 2007 from the Faculty of Engineering, University of Waterloo. Dr. Shen is a registered Professional Engineer of Ontario, Canada. He is a Fellow of the Engineering Institute of Canada and the Canadian Academy of Engineering and a Distinguished Lecturer of the IEEE Vehicular Technology and Communications Societies.

Mischa Dohler (S'01–M'03–SM'07–F'14) is currently a Full Professor of wireless communications with King's College London, London, U.K. He is also the Head of the Centre for Telecommunications Research, and a Cofounder and member of the Board of Directors of the smart city pioneer Worldsensing. He has contributed to numerous wireless broadband and IoT/M2M standards, holds a dozen patents, chaired numerous conferences, and published more than 160 refereed transactions, conference papers and books. He has a citation h-index of 34. He acts as a policy, technology, and entrepreneurship adviser, examples being Richard Branson's Carbon War Room, the House of Lords U.K., the EPSRC ICT Strategy Advisory Team, the European Commission, ISO Smart City working group, and various start-ups. Mr. Dohler is a Distinguished Lecturer of the IEEE. He serves as the Editor-in-Chief of the *Transactions on Emerging Telecommunications Technologies*. He is a frequent keynote, panel and tutorial speaker.

Chuang Lin (SM'04) received the Ph.D. degree in computer science from Tsinghua University, Beijing, China, in 1994. He is currently a Professor with the Department of Computer Science and Technology, Tsinghua University, Beijing, China. He is an Honorary Visiting Professor with The University of Bradford, Bradford, U.K. His current research interests include computer networks, performance evaluation, network security analysis, and Petri net theory and its applications. He has published more than 500 papers in research journals and IEEE conference proceedings in these areas and has published five books. Dr. Lin serves as the Technical Program Vice Chair for the Tenth IEEE Workshop on Future Trends of Distributed Computing Systems (FTDCS 2004) and as the General Chair for ACM SIGCOMM Asia workshop 2005 and the 2010 IEEE International Workshop on Quality of Service (IWQoS 2010). He also serves as the Associate Editor for IEEE TRANSACTIONS ON VEHICULAR TECHNOLOGY and as the Area Editor for *Journal of Computer Networks*.

Zhangdui Zhong is currently with Beijing Jiaotong University, Beijing, China, where he is a Professor, an Advisor of Ph.D. candidates, the Dean of the School of Computer and Information Technology, and a Chief Scientist of the State Key Laboratory of Rail Traffic Control and Safety with Beijing Jiaotong University. He is also the Director of the Innovative Research Team of the Chinese Ministry of Education, and a Chief Scientist of the Chinese Ministry of Railways. His research has been widely used in the railway engineering, such as Qinghai–Xizang railway, Datong–Qinhuangdao Heavy Haul railway, and many high-speed railway lines of China. His research interests include wireless communications for railways, control theory and techniques for railways, and GSM-R systems. He received the MaoYiSheng Scientific Award of China, the Zhan–TianYou Railway Honorary Award of China, and the Top 10 Science/Technology Achievements Award of Chinese Universities. Dr. Zhong is currently an executive council member of Radio Association of China and a Deputy Director of the Radio Association of Beijing.